Enhancing GAT-3 in thalamic astrocytes promotes resilience to brain injury in rodents

Cho, F.S.; Vainchtein, I.D.; Voskobiynyk, Y.; Morningstar, A.R.; Aparicio, F.; Higashikubo, B.; Ciesielska, A.; Broekaart, D.W.M.; Anink, J.J.; van Vliet, E.A.; Yu, X.; Khakh, B.S.; Aronica, E.; Molofsky, A.V.; Paz, Jeanne T

DOI
10.1126/scitranslmed.abj4310

Publication date
2022

Document Version
Final published version

Published in
Science translational medicine

BRAIN INJURY

Enhancing GAT-3 in thalamic astrocytes promotes resilience to brain injury in rodents

Frances S. Cho[1,2,3], Ilia D. Vainchtein[4], Yuliya Voskobiynyk[1], Allison R. Morningstar[1], Francisco Aparicio[2,3], Bryan Higashikubo[1], Agnieszka Ciesielska[1], Diede W. M. Broekaart[5], Jasper J. Anink[5], Erwin A. van Vliet[5,6], Xinzhu Yu[7,8]†, Baljit S. Khakh[7,8], Eleonora Aronica[5,9], Anna V. Molofsky[2,4,10], Jeanne T. Paz[1,2,3,10]*

Inflammatory processes induced by brain injury are important for recovery; however, when uncontrolled, inflammation can be deleterious, likely explaining why most anti-inflammatory treatments have failed to improve neurological outcomes after brain injury in clinical trials. In the thalamus, chronic activation of glial cells, a proxy of inflammation, has been suggested as an indicator of increased seizure risk and cognitive deficits that develop after cortical injury. Furthermore, lesions in the thalamus, more than other brain regions, have been reported in patients with viral infections associated with neurological deficits, such as SARS-CoV-2. However, the extent to which thalamic inflammation is a driver or by-product of neurological deficits remains unknown. Here, we found that thalamic inflammation in mice was sufficient to phenocopy the cellular and circuit hyperexcitability, enhanced seizure risk, and disruptions in cortical rhythms that develop after cortical injury. In our model, downregulation of the GABA transporter GAT-3 in thalamic astrocytes mediated this neurological dysfunction. In addition, GAT-3 was decreased in regions of thalamic reactive astrocytes in mouse models of cortical injury. Enhancing GAT-3 in thalamic astrocytes prevented seizure risk, restored cortical states, and was protective against severe chemoconvulsant-induced seizures and mortality in a mouse model of traumatic brain injury, emphasizing the potential of therapeutically targeting this pathway. Together, our results identified a potential therapeutic target for reducing negative outcomes after brain injury.

INTRODUCTION

Neuroinflammation that occurs after brain lesions such as traumatic brain injury (TBI) and stroke is a double-edged sword, contributing to both recovery and pathogenesis (*1*–*5*). Accordingly, most anti-inflammatory treatments have failed to prevent neurological deficits after brain injuries in clinical trials (*1*, *2*). Untangling the adaptive and maladaptive aspects of neuroinflammation is a crucial step in developing targeted treatments that could promote brain recovery without jeopardizing the adaptive aspects of the neuroinflammatory process.

Accumulating evidence suggests that the thalamus is particularly vulnerable to secondary damage, even when the initial injury occurred at a remote location. In both humans and rodent models, chronic thalamic inflammation is observed after TBI (*6*–*11*) and cortical stroke (*12*–*14*). The development of secondary and persistent thalamic inflammation—particularly gliosis—has been suggested to be an indicator of neurological dysfunction after injury, resulting in cognitive impairment (*8*) and seizure risk (*12*). In addition, thalamic lesions and/or thrombotic strokes have been reported among patients with viral infections caused by West Nile virus (*15*, *16*) and those with altered mental status following severe acute respiratory syndrome coronavirus-2 (SARS-CoV-2) infection (*17*, *18*). Mice intranasally infected with SARS-CoV-2 have high viral antigen presence in the thalamus compared to other brain regions (*19*). Because the thalamus plays a central role in cognition, sleep, and seizures in humans and rodents (*20*–*25*), it is well positioned to be involved in diverse neurological deficits observed across insults, such as cognitive impairments, sleep disruption, and epileptogenesis (*6*, *26*, *27*). Thalamic astrogliosis—in which astrocytes become reactive and undergo changes that affect neuronal function (*5*, *28*–*33*)—has been observed in both humans and rodents after cortical injuries (*9*–*13*).

Here, we sought to determine the extent to which thalamic astrogliosis is a driver or bystander of neurological dysfunction and whether this process could be therapeutically targeted. To this end, we developed a mouse model of thalamic astrogliosis and investigated its effects on local neurons, microcircuits, and cortical states associated with cognition.

RESULTS

Thalamic astrogliosis is observed in postmortem human tissue with a history of cortical injury and in mouse models of cortical injury

Human imaging studies in patients with mild TBI have suggested that the chronic thalamic gliosis that develops secondarily after cortical lesions is an indicator of cognitive dysfunction (*6*). To investigate

[1]Gladstone Institute of Neurological Disease, San Francisco, CA 94158, USA. [2]Neuroscience Graduate Program, University of California, San Francisco, San Francisco, CA 94158, USA. [3]Department of Neurology, University of California, San Francisco, San Francisco, CA 94158, USA. [4]Department of Psychiatry/Weill Institute for Neurosciences, University of California, San Francisco, San Francisco, CA 94158, USA. [5]Amsterdam UMC location University of Amsterdam, Department of (Neuro) Pathology, Amsterdam Neuroscience, Meibergdreef 9, Amsterdam 1105 AZ, Netherlands. [6]Swammerdam Institute for Life Sciences, Center for Neuroscience, University of Amsterdam, Amsterdam 1098 XH, Netherlands. [7]Department of Physiology, David Geffen School of Medicine, University of California, Los Angeles, Los Angeles, CA 90095, USA. [8]Department of Neurobiology, David Geffen School of Medicine, University of California, Los Angeles, Los Angeles, CA 90095, USA. [9]Stichting Epilepsie Instellingen Nederland (SEIN), Heemstede 2103 SW, Netherlands. [10]Kavli Institute for Fundamental Neuroscience, University of California, San Francisco, San Francisco, CA 94158, USA.
*Corresponding author. Email: jeanne.paz@gladstone.ucsf.edu
†Present address: Department of Molecular and Integrative Physiology, Beckman Institute, University of Illinois at Urbana-Champaign, Urbana, IL 61801, USA.

the role of astrogliosis in cortical stroke and TBI, we first performed immunostaining for the astrocytic marker glial fibrillary acidic protein (GFAP)—a molecular marker of many types of reactive astrocytes (*28*)—in postmortem thalamic and perilesional cortical tissue obtained from human brains with a history of ischemic stroke or TBI; a subset of subjects also had a history of epilepsy (2 of 7 subjects had epilepsy before injury, and 3 of 7 subjects developed epilepsy after injury) (Fig. 1 and tables S1 and S2). The thalamus and perilesional cortex of subjects with stroke or TBI exhibited discrete GFAP-positive cells with astrocyte-like morphology, compared to the dim, diffuse GFAP labeling in control subjects (Fig. 1A). Putative astrocyte morphology ranged from resting (Fig. 1A; cortex, control, inset) to reactive, featuring somatic hypertrophy and thick processes (Fig. 1A; thalamus and cortex, stroke, inset). These changes were evident both acutely and years after stroke or TBI and were supported by a semiquantitative analysis of GFAP immunoreactivity (table S2). Similarly, in two mouse models of injury—unilateral photothrombotic stroke or controlled cortical impact in the somatosensory cortex (a model of TBI)—GFAP was elevated in the thalamus, without gross hippocampal damage (Fig. 1B), in agreement with previous findings (*10*–*13*, *34*).

Viral transduction of thalamic astrocytes induces persistent reactive astrocytes

To generate reactive astrocytes in the thalamus, we injected an adeno-associated viral (AAV) construct expressing enhanced green fluorescent protein (eGFP) from a truncated portion of the GFAP promoter (AAV2/5-Gfa104-eGFP) (*35*) unilaterally in the ventrobasal (VB) somatosensory thalamus (Fig. 1C and fig. S1, A and B). This paradigm was originally developed to selectively transduce hippocampal astrocytes and render them reactive, as determined by hypertrophy and increased GFAP expression (*35*), although the molecular mechanisms of virus-induced reactive astrogliosis remain unknown.

To characterize the effects of the viral transduction on thalamic astrocytes, we assessed immunohistochemical, morphological, and transcriptomic features of astrocytes 3 weeks after viral transduction. GFAP was increased in the thalamus ipsilateral to injection (Fig. 1D), consistent with the work in the hippocampus (*35*). The location of thalamic astrogliosis in our model was similar to that observed in rodent models of cortical injuries (Fig. 1B). The increase in GFAP in the viral transduction model persisted for at least 9 months, specifically in the ipsilateral thalamus but not in other brain regions (fig. S1C). Thus, the viral transduction model recapitulated two key features of astrogliosis after cortical injury—the specific location within the dorsal thalamus and the chronic presence of reactive astrocytes in the thalamus (*10*).

To evaluate astrocyte morphology, we used an EAAT2-tdTomato transgenic reporter mouse line (*36*), which enabled sparse labeling and tracing of individual thalamic astrocytes (Fig. 1E). Using Sholl analysis to assess arborization of astrocytic processes (*37*), we observed somatic hypertrophy and a reduction in process branching in eGFP-positive astrocytes ipsilateral to viral injection (eGFP-positive/tdT-positive) relative to eGFP-negative/tdT-positive astrocytes (Fig. 1F). Thus, viral transduction of thalamic astrocytes recapitulates morphological features of reactive astrogliosis (*32*, *35*, *38*).

We next performed transcriptomic profiling of virally transduced thalamic astrocytes acutely isolated by fluorescence-activated cell sorting (FACS; Fig. 1, G and H, and fig. S2). Hierarchical clustering of FACS-isolated samples revealed that eGFP-positive astrocytes, which represented ~18% of astrocytes isolated from the thalamus, were distinct from their eGFP-negative counterparts (fig. S3, A to C). We found robust up-regulation of canonical reactivity genes *Gfap*, *Vim*, *CD44*, and *Serpina3n* (*31*, *33*) in eGFP-positive astrocytes (Fig. 1H). Comparing this transcriptomic profile with a published analysis of reactive astrocytes revealed up-regulation of "pan-reactive" astrocyte genes (*31*), although there was no bias toward the subsets of reactive astrocyte genes that were selectively induced by lipopolysaccharide injection or ischemic stroke (middle cerebral artery occlusion model) in that study (*31*) (fig. S3D). Last, we found alterations in multiple genes related to astrocytic modulation of glutamate and γ-aminobutyric acid (GABA) (Fig. 1H), pinpointing molecular features of reactive astrocytes that might affect neural activity. Given that viral transduction of thalamic astrocytes reproducibly induces immunohistochemical, morphological, and transcriptomic features of astrocyte reactivity observed across models (*28*, *32*, *35*, *38*), hereon, we refer to virally transduced astrocytes as reactive astrocytes. Viral-induced thalamic astrogliosis did not lead to abnormalities in standard assays of spontaneous locomotion, anxiety, olfaction, nociception, context-dependent learning, and grooming 3 weeks after injection (fig. S4).

Reactive astrocytes enhance intrathalamic microcircuit excitability

The effects of reactive astrocytes on local microcircuit excitability were assessed in acute brain slices that preserve the connectivity between VB thalamus and the reticular thalamic nucleus (nRT). We focused on the VB-nRT microcircuit because (i) VB thalamus—the center of viral transduction—showed the strongest and most persistent astrogliosis over time (fig. S1); (ii) the VB-nRT connections can be maintained in slices and reliably generate circuit oscillations, unlike connections between nRT and other thalamic nuclei; and (iii) multiunit activity in VB thalamus is a proxy for the strength of the oscillatory activity in the VB-nRT microcircuit (*39*–*43*).

Electrical stimulation was delivered in the internal capsule, which contains corticothalamic and thalamocortical axons, and the resulting multiunit activity was recorded 3 weeks after induction of reactive astrocytes (Fig. 2). Stimulation of the internal capsule produced robust multiunit activity, characterized by an immediate "direct response," due to direct activation of corticothalamic axons and/or retrograde activation of thalamocortical neurons, followed by a "delayed response," characterized by repeated action potential (AP) bursts (Fig. 2, A to C), characteristic of the reciprocal VB-nRT oscillatory circuit activity (*39*–*43*). Thalamic slices with astrogliosis exhibited an augmented delayed response characterized by more bursts and longer circuit oscillations (Fig. 2D). Beyond the site of maximal responsiveness in each slice, we also examined the spatial and temporal synchrony of neural activity across all recording sites. Evoked oscillatory activity in thalamic slices with astrogliosis had higher oscillation indices (Fig. 2, B and E) (*39*, *44*), although the spatial extent of the direct response was not altered, suggesting that astrogliosis enhanced the rhythmogenic properties of the intrathalamic microcircuit across a larger region.

Reactive astrocytes facilitate low-threshold calcium spikes in thalamocortical neurons by increasing extrasynaptic tonic inhibition

To determine how reactive astrocytes cause hyperexcitability in the VB-nRT microcircuit, we investigated cellular excitability and synaptic

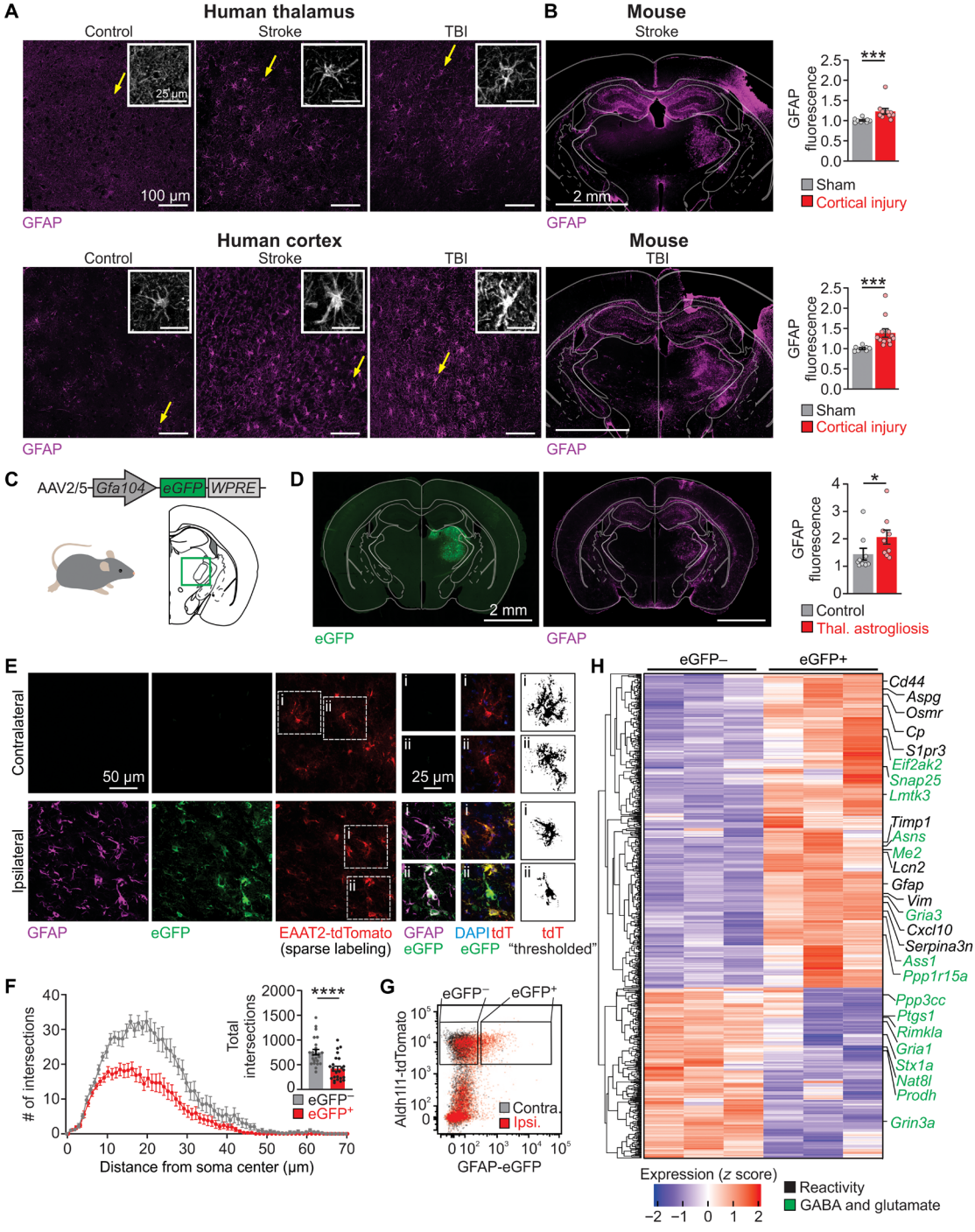

Fig. 1. Thalamic astrogliosis is a consistent feature of cortical lesions, recapitulated by viral-mediated activation. (**A**) GFAP immunofluorescence in postmortem thalamus and perilesional cortex from human subjects with a history of ischemic stroke or TBI, and age-matched controls, representative of three control subjects, three subjects with stroke, and four subjects with TBI. Insets: magnification of GFAP$^+$ cells with astrocyte-like morphology (putative astrocytes, yellow arrows). (**B**) GFAP immunofluorescence in mouse models of photothrombotic stroke and controlled cortical impact. Right: thalamic GFAP fluorescence ratios between ipsilateral and contralateral regions. Stroke: Mann-Whitney *U* test, ***$P = 0.0002$. Sham: $n = 9$ mice; Stroke: $n = 10$ mice. TBI: Mann-Whitney *U* test, ***$P = 0.0002$. Sham: $n = 7$ mice; TBI: $n = 12$ mice. (**C**) Viral induction of unilateral thalamic astrogliosis [brain schematic adapted from (*76*)]. (**D**) Immunofluorescence 3 weeks after astrogliosis induction. GFAP immunofluorescence quantified as in (B). Mann-Whitney *U* test, *$P = 0.019$. $n = 9$ mice per group. Quantification in other brain regions shown in fig. S1. (**E**) Representative images of GFAP, eGFP, tdTomato, and 4′,6-diamidino-2-phenylindole (DAPI) fluorescence in thalamic astrocytes contralateral and ipsilateral to viral transduction of astrocytes in EAAT2-tdTomato reporter mice. (**F**) Sholl analysis of thalamic astrocytes. Inset: Total number of intersections. Mann-Whitney *U* test, ****$P < 0.0001$. $n = 25$ astrocytes per condition. (**G**) Flow plot of thalamic astrocytes, ipsilateral and contralateral to site of viral transduction in Aldh1l1-tdTomato reporter mice. Gates indicate sorting strategy detailed in fig. S2. (**H**) Differentially expressed genes in ipsilateral eGFP$^+$ versus contralateral eGFP$^-$ thalamic astrocytes ($P_{adjusted} < 0.05$), highlighting genes related to astrocyte reactivity (*31*) and astrocyte modulation of glutamate and GABA (*54*, *77*) on the right. Heatmap including ipsilateral eGFP$^-$ in fig. S3.

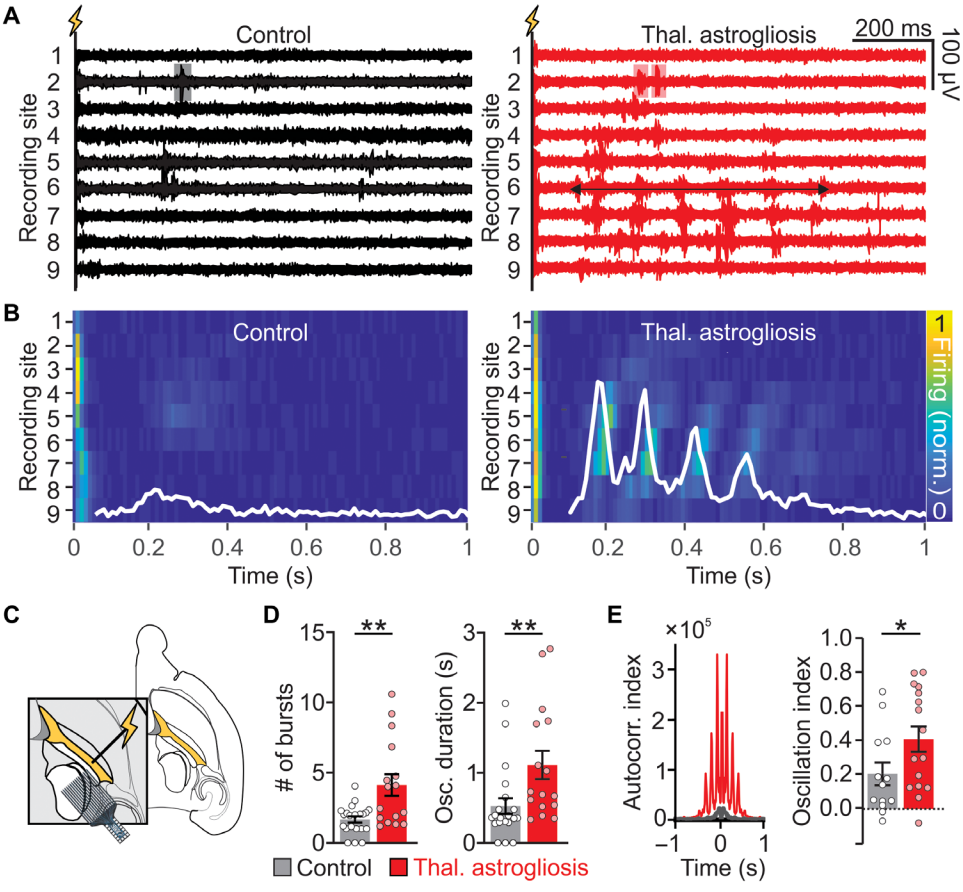

Fig. 2. Viral-mediated thalamic astrogliosis enhances intrathalamic circuit rhythmogenesis. (**A**) Representative intrathalamic multiunit activity evoked by stimulation of the internal capsule (lightning bolt) in thalamic slices, as schematized in (C). Only 9 of 16 channels are shown for clarity. Shaded boxes highlight bursts (clusters of ≥3 spikes), and the horizontal arrow indicates a sustained circuit oscillation (clusters of ≥2 bursts). (**B**) Peristimulus time histograms of recordings shown in (A). Color represents multiunit activity normalized to maximal firing in each slice. White traces represent the spatial summation of firing activity across all recording sites and all trials within each slice during the delayed response (excluding the first 150 ms of direct response). (**C**) Schematic of multiunit activity recordings in thalamic slices after electrical stimulation of the internal capsule (yellow). Probe schematic adapted from NeuroNexus, brain schematic adapted from (*76*). (**D**) Quantification of bursts and circuit oscillations, as shown in (A). Each dot represents the site with maximal multiunit activity in each slice from $n = 13$ Control and $n = 16$ thalamic astrogliosis mice (1 slice per mouse; 20 evoked responses averaged per slice). Mann-Whitney *U* test; $^{**}P = 0.007$ (bursts) and $^{**}P = 0.003$ (oscillations). (**E**) Left: autocorrelation analyses of multiunit activity in the delayed response from (B). Multiunit activity is summed across all recording sites and all trials within a slice. Right: oscillation index calculated for the first peak of the autocorrelated signal. Mann-Whitney *U* test, $^{*}P < 0.05$. $n = 13$ Control, $n = 16$ thalamic astrogliosis mice.

function in excitatory and inhibitory neurons in thalamic brain slices (tables S3 to S8) (*12*, *45*, *46*). Thalamocortical neurons in VB thalamus from mice with thalamic astrogliosis exhibited hyperpolarized AP threshold (Fig. 3, A and B) and no difference in the resting membrane potential (Fig. 3C). The difference in AP threshold was abolished when membrane potential was held at −75 mV in both groups (table S4). Furthermore, the postinhibitory rebound low-threshold calcium spike (LTS), mediated by T-type Ca^{2+} currents (*47*), occurred at more hyperpolarized membrane potentials (Fig. 3D) and was accompanied by enhanced AP firing (fig. S5, A to C). T-type Ca^{2+} current properties were similar in thalamocortical neurons from both groups (table S5), as was the hyperpolarization-activated depolarizing sag potential (fig. S5, D to G).

In mice with thalamic astrogliosis, thalamocortical neurons showed a threefold increase in extrasynaptic GABA type A receptor ($GABA_AR$)–mediated current (hereon referred to as tonic GABA current or I_{TONIC}) (Fig. 3E) but no change in the frequency or biophysical properties of spontaneous inhibitory and excitatory synaptic currents (Fig. 3F and table S6). $GABA_AR$ antagonist picrotoxin normalized the AP threshold, LTS threshold, and rebound burst AP firing (Fig. 3, B to D, and fig. S5C). In contrast with thalamocortical neurons, nRT neurons showed no change in intrinsic membrane excitability (table S7) or in spontaneous synaptic currents (table S8).

Thalamic reactive astrocytes enhance seizure risk in mice via tonic inhibition in thalamocortical neurons

Given that enhanced I_{TONIC} in the rodent thalamus has been implicated in hyperexcitability and seizures in genetic and pharmacological models of epilepsies (*46*, *48*), we asked whether thalamic astrogliosis—which increased I_{TONIC} in adult wild-type mice (Fig. 3E)—led to heightened seizure susceptibility in mice. Three weeks after induction of thalamic astrogliosis, a low dose of the proconvulsive agent pentylenetetrazol [PTZ; 5 mg/kg, intraperitoneally (i.p.)] was sufficient to induce epileptiform discharges associated with behavioral freezing in mice with thalamic astrogliosis but not in control mice (Fig. 4, A to D). Epileptiform discharges were prominent in the primary somatosensory cortex S1, a major recipient of inputs from VB thalamus (*49*), and generalized to other cortical areas (fig. S6A). These epileptiform discharges were similar to those reported in rodent models of epilepsies in terms of peak frequency and generalization (*43*, *46*, *50*). Increased seizure susceptibility persisted for at least 7 months (fig. S6B), consistent with the persistent thalamic astrogliosis (fig. S1). Mice in which astrocytes were transduced with a low titer of the same viral construct [previously shown to not induce astrocyte reactivity (*35*)] did not exhibit enhanced seizure risk (fig. S6C). Mice with thalamic astrogliosis also had a heightened response to kainic acid (10 mg/kg, i.p.) (Fig. 4, E to G, and fig. S6D). Together, these results show that unilateral induction of reactive astrocytes in the thalamus enhances susceptibility to both nonconvulsive and generalized tonic-clonic seizures, as assessed by proconvulsive agents that act through different mechanisms (GABA and glutamate).

In the thalamus, δ-subunit–containing extrasynaptic $GABA_ARs$ generate I_{TONIC} (*45*, *46*, *48*). Thus, to investigate whether preventing

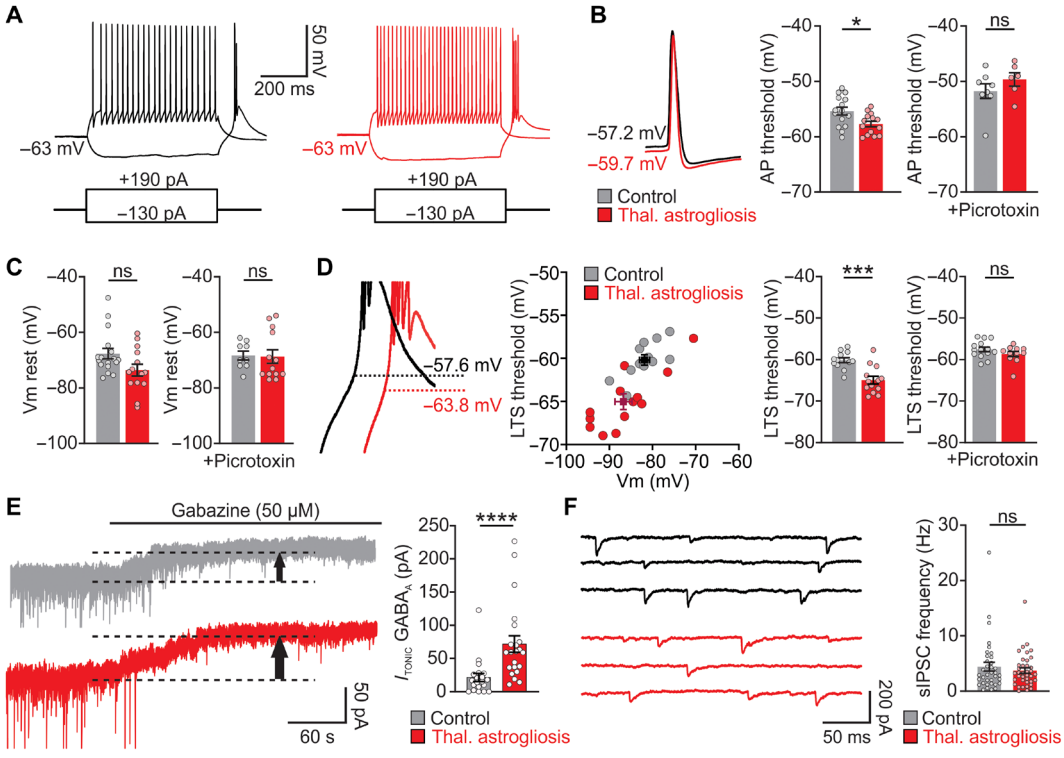

Fig. 3. Viral-mediated thalamic astrogliosis boosts cellular excitability via extrasynaptic GABA$_A$R-mediated tonic inhibition. (**A**) Representative whole-cell recordings showing response to hyperpolarizing and depolarizing intracellular current injections. (**B**) Left: Overlay of action potentials (APs) from two representative neurons. Right: AP generation threshold in the presence or absence of picrotoxin (50 μM). No-picrotoxin condition: Mann-Whitney *U* test, **P* = 0.02; Control: *n* = 17 cells (from eight slices, four mice); thalamic astrogliosis: *n* = 14 cells (from seven slices, five mice). Picrotoxin condition: *P* = 0.28; Control: *n* = 9 cells (from five slices, three mice). Thalamic astrogliosis: *n* = 13 cells (from nine slices, five mice). ns: not significant. (**C**) Resting membrane potentials of thalamocortical neurons. No-picrotoxin condition: Mann-Whitney *U* test, *P* = 0.053. Picrotoxin condition: Mann-Whitney *U* test, *P* = 0.52. See (A) for sample size. (**D**) Left: Overlay of the hyperpolarization-induced rebound burst from two representative neurons. Center: Threshold for the T-type Ca^{2+}-mediated low threshold spike (LTS), plotted as a function of the pre-pulse hyperpolarized membrane potential after current injection. Black and burgundy crosses indicate means ± SEM for membrane potential and LTS threshold. Right: LTS threshold. No-picrotoxin condition: Mann-Whitney *U* test, ****P* = 0.0005. Control: *n* = 12 cells (from seven slices, four mice). Thalamic astrogliosis: *n* = 12 cells (from seven slices, five mice). Picrotoxin condition: *P* = 0.36. Control: *n* = 13 cells (from nine slices, four mice). Thalamic astrogliosis: *n* = 11 cells (seven slices, five mice). (**E**) Representative whole-cell voltage-clamp recordings. Gabazine (50 μM) was bath-applied to isolate I_{TONIC}, measured by the shift in baseline holding current (black arrow). Mann-Whitney *U* test, *****P* < 0.0001. Control: *n* = 20 cells (from 20 slices, 10 mice); thalamic astrogliosis: *n* = 22 cells (from 22 slices, 11 mice). (**F**) Representative spontaneous phasic GABA$_A$ currents. Mann-Whitney *U* test, *P* = 0.88. Control: *n* = 36 cells (from 36 slices, 14 mice); thalamic astrogliosis: *n* = 40 cells (from 40 slices, 16 mice).

the increase in I_{TONIC} could prevent astrogliosis-induced seizure risk, we conditionally deleted the GABA$_A$R δ subunit (δ-GABA$_A$R) unilaterally in thalamocortical neurons of adult *Gabrd*$^{Fl/Fl}$ mice (*51*) (Fig. 4H). Thalamic astrogliosis did not increase I_{TONIC} in thalamocortical neurons in these mice (Fig. 4I) and did not increase seizure risk (Fig. 4J), indicating that astrogliosis-induced increase in I_{TONIC} in thalamocortical neurons is necessary for the development of hyperexcitability.

Enhancing GAT-3 in thalamic astrocytes prevents astrogliosis-induced seizure risk and cortical rhythm perturbations in mice

Astrocytes take up GABA from the extracellular space, mainly via the GABA transporters GAT-1 and GAT-3 (*46*, *52*, *53*). Given the alterations in multiple genes linked to GAT regulation (*54*) in our transcriptomic study (Fig. 1H), we investigated whether the expression of these transporters was altered in reactive astrocytes. Three weeks after viral induction of astrogliosis, GAT-3 expression was reduced in the ipsilateral thalamus, and *Slc6a11* transcripts (encoding GAT-3) were reduced in reactive astrocytes (Fig. 5, A to C). The reduction of GAT-3 mRNA was specific to eGFP-transfected reactive astrocytes (Fig. 5C and fig. S7, A and B), and there was no evidence of compensatory changes in GAT-1 mRNA (fig. S7, C and D). Enhancing GAT-3 expression unilaterally in thalamic astrocytes by transducing mice with an astrocyte-specific viral construct (AAV2/5-GfaABC$_1$D-GAT3) (*54*) at the same time as the induction of thalamic astrogliosis (Fig. 5D) counteracted the enhanced I_{TONIC} in thalamocortical neurons (Fig. 5E) and protected mice from increased seizure risk (Fig. 5F).

We next investigated whether induction of reactive astrocytes in the thalamus could initiate long-term changes in cortical rhythms. Seven weeks after induction of thalamic astrogliosis, spectral analysis revealed a unilateral reduction in the sigma (12 to 15 Hz) and gamma (30 to 75 Hz) power but not in total power (Fig. 6, A to C, and table S9). The reduction of sigma power was specific to the 12-hour light cycle, whereas the reduction of gamma power was specific to the 12-hour dark cycle (table S9). Enhancement of GAT-3 expression in thalamic astrocytes protected from the loss of sigma and gamma power in the ipsilateral cortex (Fig. 6D and table S9).

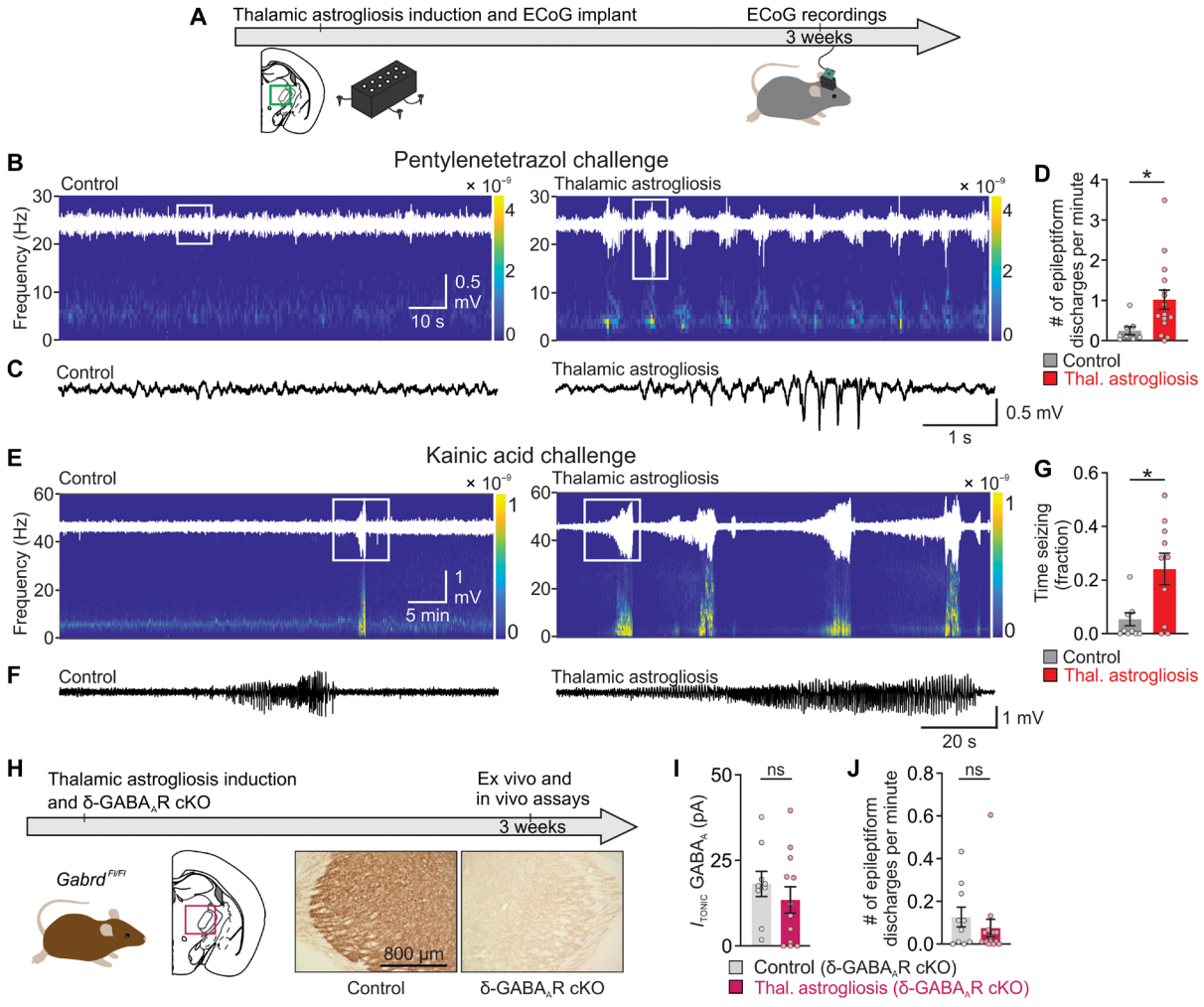

Fig. 4. Conditional deletion of the extrasynaptic GABA$_A$R δ-subunit (δ-GABA$_A$R-cKO) in thalamocortical neurons prevents thalamic astrogliosis–induced seizure risk. (**A**) Experimental timeline of electrocorticography (ECoG) recordings. (**B** and **E**) Representative ECoG recordings from ipsilateral primary somatosensory cortex (S1) after intraperitoneal injection of pentylenetetrazol (PTZ, 5 mg/kg; B) or of kainic acid (10 mg/kg; E), with raw ECoG traces (white) overlaid onto corresponding spectrograms. (**C** and **F**) Enlargement of ECoG traces in boxed areas in (B) and (E). (**D**) Frequency of epileptiform discharges in ipsilateral S1 ECoG in the PTZ challenge experiment. Mann-Whitney *U* test: $^*P = 0.013$. Control, $n = 8$ mice; thalamic astrogliosis, $n = 15$ mice. (**G**) Time spent seizing in response to kainic acid challenge. Mann-Whitney *U* test, $^*P = 0.025$. Control: $n = 10$ mice; thalamic astrogliosis: $n = 10$ mice. (**H**) Unilateral, conditional deletion of the extrasynaptic GABA$_A$R δ-subunit (δ-GABA$_A$R-cKO) in thalamocortical neurons (TC) via viral Cre-mediated (AAV2/5-CaMKIIα-mCherry-Cre) recombination in *Gabrd*$^{Fl/Fl}$ mice. Timeline (top) and 3,3′-Diaminobenzidine (DAB) labeling in thalamic sections (bottom). (**I**) Quantification of I_{TONIC} in thalamocortical neurons in thalamic ex vivo slices from *Gabrd*$^{Fl/Fl}$ mice. Mann-Whitney *U* test, $P = 0.42$. Control δ-GABA$_A$R-cKO (intrathalamic transduction of thalamocortical neurons with AAV2/5-CaMKIIα-mCherry-Cre in mice without astrogliosis): $n = 9$ cells (from nine slices, five mice); thalamic astrogliosis δ-GABA$_A$R-cKO (intrathalamic transduction of thalamocortical neurons with AAV2/5-CaMKIIα-mCherry-Cre in mice with astrogliosis): $n = 12$ cells (from 12 slices, five mice). (**J**) Epileptiform discharges from ipsilateral S1 in response to PTZ challenge (5 mg/kg) in *Gabrd*$^{Fl/Fl}$ mice with and without thalamic astrogliosis. Mann-Whitney *U* test, $P = 0.37$. Control δ-GABA$_A$R-cKO: $n = 10$ mice; thalamic astrogliosis δ-cKO: $n = 14$ mice.

Enhancing GAT-3 in thalamic astrocytes reduces chemoconvulsant-induced seizure severity and mortality in a mouse model of cortical injury

We investigated whether similar reductions of thalamic GAT-3 transcripts occurred, and whether enhancing thalamic GAT-3 would confer resilience, in a mouse model of cortical injury. First, we performed 10x Visium Spatial Transcriptomics on tissue obtained from mice after TBI, stroke, or a sham procedure (Fig. 7 and fig. S8). Portions of the thalamus exhibited a higher number of *Gfap* transcripts and other markers of astrogliosis 6 weeks after stroke or TBI (Fig. 7, A to C, and fig. S9). Elevated *Gfap* expression was associated with reduced *Slc6a11* expression in the thalamus (Fig. 7, D and E), whereas no correlation was found in the cortex (fig. S9).

Enhancing GAT-3 in thalamic astrocytes ipsilateral to cortical TBI (fig. S10A) increased survival after PTZ challenge; 5 of 12 TBI mice died after the PTZ challenge, whereas all 10 TBI mice that received astrocytic GAT-3 treatment survived (fig. S10B). Furthermore, GAT-3 treatment resulted in reduced seizure severity after TBI (fig. S10, C and D).

We next investigated GAT-3 expression in human brain samples. Using a recently described method to deconvolute cell type–specific and brain region–specific transcriptional signatures from

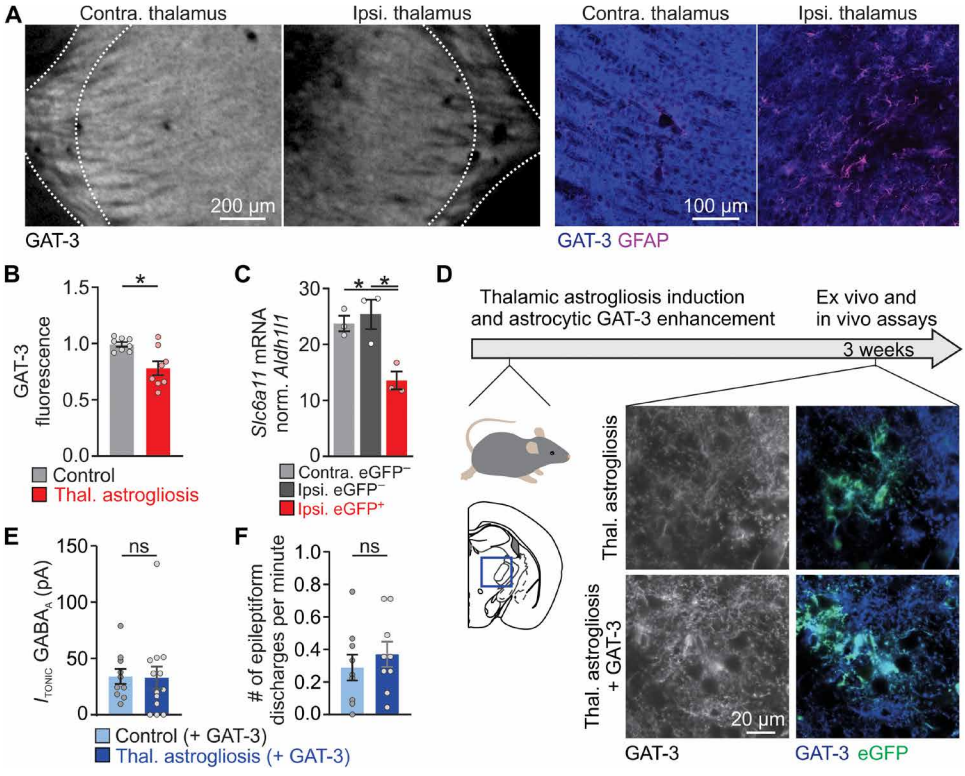

Fig. 5. Enhancing GAT-3 in thalamic astrocytes prevents astrogliosis-induced tonic inhibition in neurons and seizure risk. (**A**) GAT-3 immunofluorescence in mouse coronal brain sections (left) and confocal images of GAT-3 and GFAP colocalization in VB thalamus (right), 3 weeks after unilateral thalamic astrogliosis induction. (**B**) GAT-3 immunofluorescence ratio between regions ipsilateral and contralateral to thalamic astrogliosis, 3 weeks after induction. Mann-Whitney *U* test, $^*P = 0.028$; $n = 8$ mice per group. (**C**) qPCR analysis of *Slc6a11* expression (encoding GAT-3), normalized to *Aldh1l1* expression in astrocytes FACS-isolated from contralateral and ipsilateral VB thalamus of Aldh1l1-tdTomato mice, 3 weeks after thalamic astrogliosis induction. Sorting strategy detailed in fig. S2. One-way ANOVA, $^*P = 0.01$; Shapiro-Wilk normality test, $P > 0.05$, Tukey's post hoc tests, $^*P = 0.012$ and $^*P = 0.024$; $n = 3$ mice. (**D**) Increased GAT-3 expression in thalamic astrocytes was achieved by transducing thalamic astrocytes with AAV2/5-GfaABC$_1$D-GAT3-mCherry (*54*) in adult mice with and without thalamic astrogliosis. Representative confocal images show GAT-3 expression in eGFP$^+$ astrocytes in mice with thalamic astrogliosis, with and without enhanced GAT-3 enhancement. (**E**) Quantification of I_{TONIC} in thalamocortical neurons from thalamic ex vivo slices, 3 weeks after GAT-3 enhancement in mice with and without thalamic astrogliosis. Mann-Whitney *U* test, $P = 0.60$. Control + GAT-3: $n = 10$ cells (from 10 slices, 7 mice); thalamic astrogliosis + GAT-3: $n = 13$ cells (from 13 slices, 9 mice). (**F**) Epileptiform discharges in response to PTZ (15 mg/kg). Mann-Whitney *U* test, $P = 0.42$. $n = 9$ mice per group.

thousands of neurotypical adult human brain samples (*55*), we found that *SLC6A11* (encoding GAT-3) was highly expressed in the thalamus-containing diencephalon relative to all genes detected in this region (Fig. 8A). Comparing the fidelity of *SLC6A11* expression to transcriptional signatures of the major brain cell types showed that *SLC6A11* expression was highly correlated to an astrocyte transcriptional signature and not to neurons, oligodendrocytes, or microglia (Fig. 8B and fig. S11), consistent with ultrastructural studies suggesting that GAT-3 is predominantly expressed in astrocytes in the rodent thalamus (*56*, *57*). We next performed immunostaining for GAT-3 in postmortem thalamic and perilesional cortical tissue obtained from human brains with a history of ischemic stroke or TBI (Fig. 8, fig, S11, and tables S1 and S2). The extent of colocalization between GAT-3 and GFAP-positive putative astrocytes varied, prominent in some cases (such as thalamus and cortex of control subject; Fig. 8, C and D) and less prominent in others (such as thalamus of stroke and TBI subject; Fig. 8C). In a blinded, semiquantitative scoring of GAT-3 intensity, thalamic samples from control subjects displayed a median score of 3 (corresponding to dense GAT-3 immunoreactivity), whereas thalamic samples from subjects with stroke or TBI displayed, respectively, a median score of 2 (moderate GAT-3) and 2.5 (moderate to dense GAT-3) (table S2). Cortical samples from control subjects and perilesional cortical samples from subjects with stroke or TBI, displayed a median score of 2 (moderate GAT-3) (table S2).

DISCUSSION

Here, we demonstrate that neuroinflammation in the mouse thalamus can drive enhanced cellular and microcircuit excitability, seizure risk, and aberrant changes in cortical states in mice. Our findings pinpoint astrocytic GAT-3 as a link between neuroinflammation and long-term network dysfunction and as a potential therapeutic target for repairing circuit dynamics and promoting resilience after brain insults characterized by secondary and persistent thalamic neuroinflammation. Although astrocyte dysfunction has been widely documented in cellular and circuit hyperexcitability in the context of epilepsy (*3*, *38*, *58*–*62*), untangling whether reactive astrocytes are a cause and/or consequence of changes in neuronal network activity remains challenging (*3*, *35*, *58*, *59*). In the thalamus, astrogliosis has been suggested to be a predictor of long-term consequences of cortical lesions, such as epilepsy and cognitive impairment (*6*, *8*, *12*, *27*). Given the role of the thalamus as a regulator of thalamocortical rhythms and higher cognitive processes, understanding whether and how reactive astrocytes in the thalamus can initiate development of pathological circuit dynamics is of broad fundamental and translational interest. To address this gap, we used a viral construct (*35*) to selectively transduce astrocytes in the mouse thalamus, recapitulating secondary thalamic astrogliosis, but in the absence of a cortical lesion.

The long-term consequences of thalamic astrogliosis included increased seizure risk and disruption of adaptive cortical rhythms in the sigma and gamma bands. These effects of thalamic astrogliosis are reminiscent of maladaptive outcomes of cortical injuries, such as increased seizure risk in mice and patients (*63*) and reduced sigma-related sleep spindles in mice (*10*, *64*) linked to sleep-wake disturbances in patients (*65*). Therefore, rather than being a mere bystander in the pathological sequelae of brain injuries, thalamic astrogliosis in mice can initiate robust, sustained aberrations in

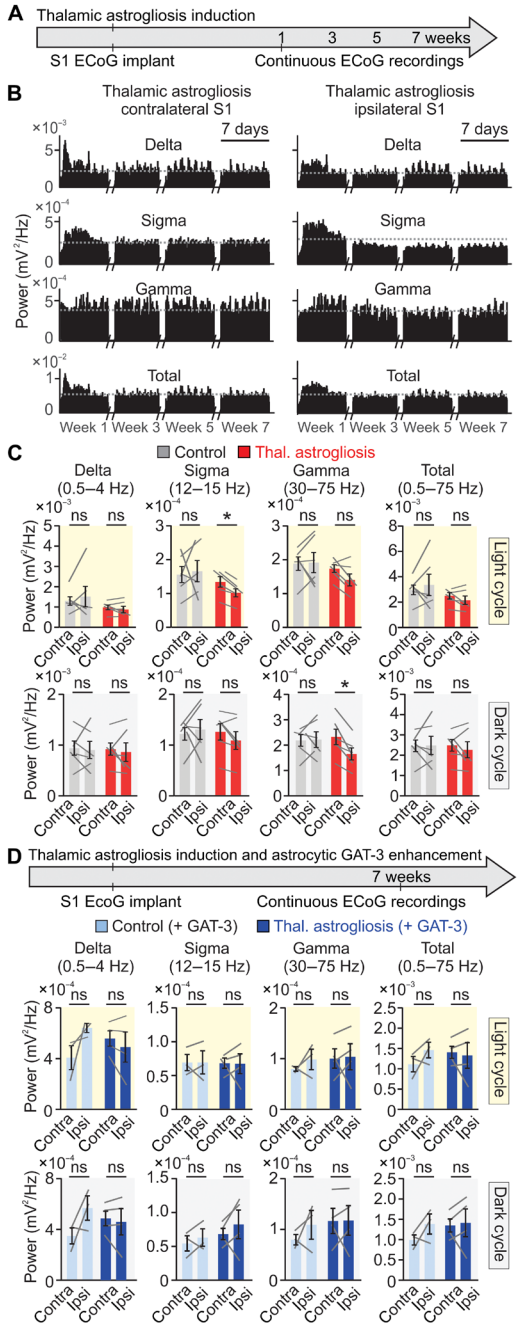

Fig. 6. Enhancing GAT-3 in thalamic astrocytes prevents astrogliosis-induced reduction in cortical sigma and gamma frequency power. (**A**) Schematic of experimental timeline. Chronic wireless ECoG from S1 was obtained bilaterally in freely behaving mice in their home cage for continuous 1-week periods, up to 7 weeks after induction of thalamic astrogliosis. (**B**) Representative plots of delta (1 to 4 Hz), sigma (12 to 15 Hz), gamma (30 to 75 Hz), and total band power (1 to 75 Hz), across weeks 1, 3, 5, and 7, obtained from a mouse with thalamic astrogliosis. Spectral analysis was performed on S1 ECoG in 1-hour bins. Horizontal lines indicate the average power of the frequency band during week 1. (**C**) Average ECoG power for each mouse, 7 weeks after thalamic astrogliosis induction, during the light (top) and dark cycle (bottom). Control: $n = 6$ mice; thalamic astrogliosis: $n = 6$ mice. (**D**) Average ECoG power for each mouse, 7 weeks after thalamic astrogliosis induction and astrocytic GAT-3 enhancement. Control + GAT-3: $n = 3$ mice; thalamic astrogliosis + GAT-3: $n = 4$ mice. See table S9 for comparison of all frequency bands. Wilcoxon matched-pairs signed rank tests, $^{*}P < 0.05$.

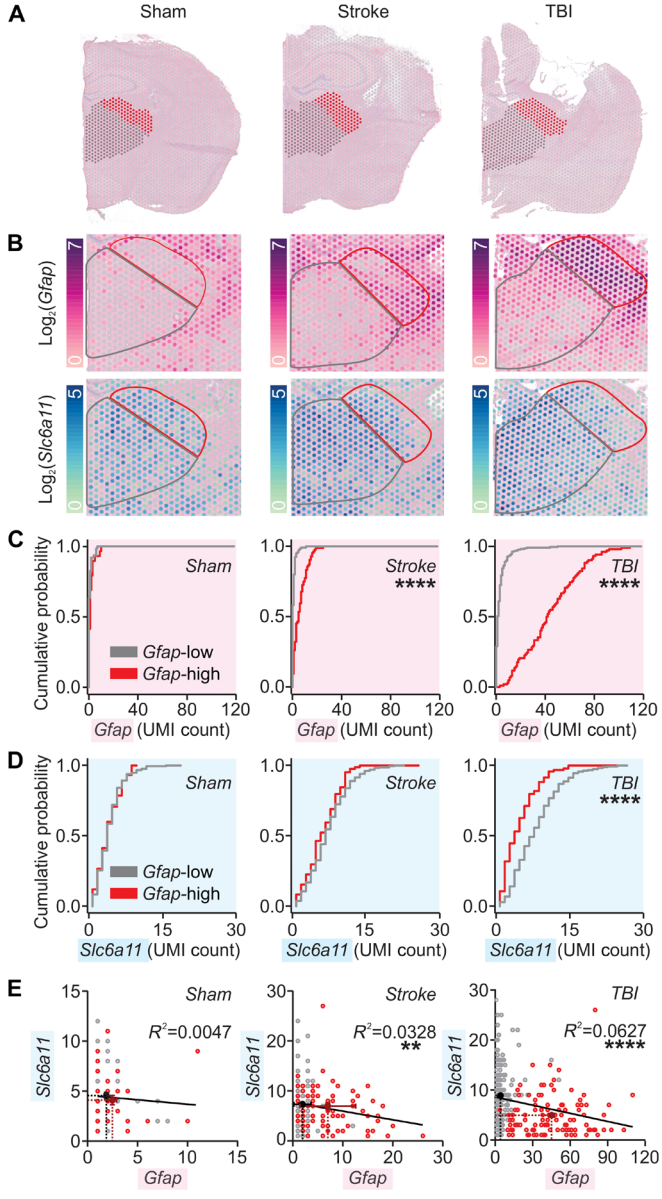

Fig. 7. Cortical injury-induced thalamic *Gfap* is negatively correlated with thalamic *Slc6a11* expression. (**A**) Hemi-brain sections from mice after sham, stroke, and TBI procedures 6 weeks after surgery overlaid with thalamic regions of interest (gray and red) analyzed with 10x Visium spatial transcriptomics and magnified in (B). (**B**) Thalamic expression of *Gfap* and *Slc6a11* transcripts. Color map indicates $\log_2$ of the detected counts of the gene's unique molecular identifier (UMI). Red and black outlines correspond to regions of interest shown in (A) and to regions with high and low *Gfap* expression in cortical injury, as detailed in (C). (**C** and **D**) Cumulative probability distribution of *Gfap* (C) or *Slc6a11* (D) expression per spot in regions indicated in (A) and (B). Kolmogorov-Smirnov test, $^{****}P < 0.0001$. All spots containing nonzero UMI counts were included. Number of spots from low- and high-*Gfap* regions, respectively, in (C): sham ($n = 63$ and 29), stroke ($n = 120$ and 84), and TBI ($n = 218$ and 102); in (D): sham ($n = 216$ and 76), stroke ($n = 237$ and 85), and TBI ($n = 277$ and 95). Adjusted $\alpha = 0.025$ for multiple comparisons. (**E**) Relationship between *Gfap* and *Slc6a11* expression. Circles represent UMI counts per spot in low-*Gfap* (gray) and high-*Gfap* (red) areas; black and burgundy crosses, and corresponding dotted lines, mark means ± SEM for low- and high-*Gfap* areas, respectively. Black lines plot the best-fit slopes and intercepts from a simple linear regression. $^{**}P = 0.0095$, $^{****}P < 0.0001$. Number of spots: sham ($n = 93$), stroke ($n = 204$), and TBI ($n = 322$). Similar analysis for cortical regions distal and proximal to injury is described in fig. S9.

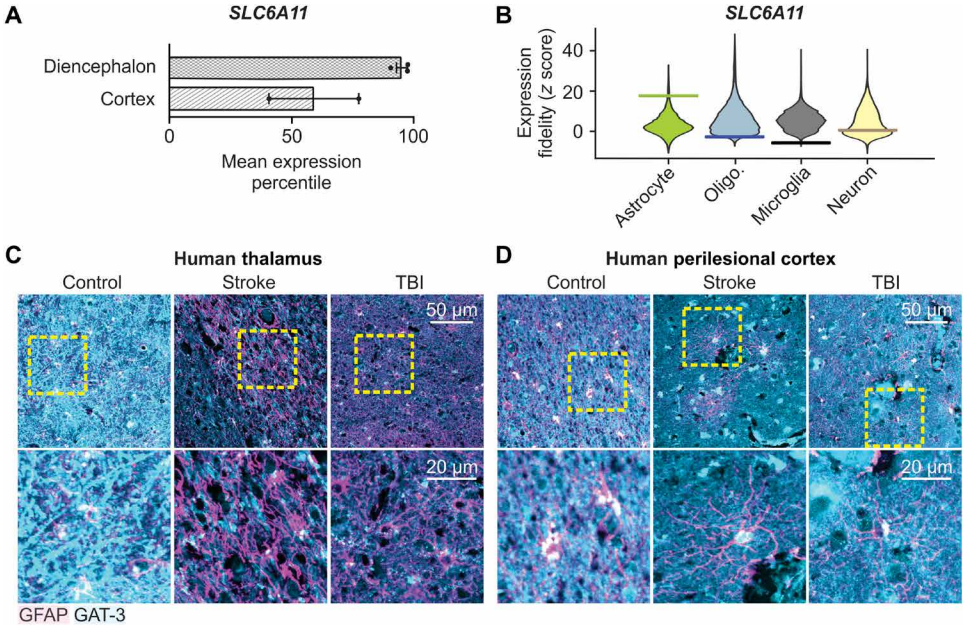

Fig. 8. Decreased GAT-3 immunoreactivity in human postmortem thalamic tissue after cortical injuries. (**A**) Mean expression percentile of *SLC6A11* gene relative to all genes in neurotypical adult human diencephalon and parietal cortex. Data obtained from (*55*) from 535 human samples. (**B**) Expression fidelity of *SLC6A11* from cell type–specific transcriptomic profiling in the adult human diencephalon compared to transcriptional signatures of major brain cell types, relative to all human genes detected in the database from (*55*). Higher fidelity indicates higher correlation of *SLC6A11* to cell type. Horizontal bar indicates *z* score for *SLC6A11* relative to that cell type (17.6, −2.8, −5.8, and 0.4 for astrocytes, oligodendrocytes, microglia, and neurons, respectively); violin plot indicates *z* score distribution for all genes detected in that cell type. (**C** and **D**) GFAP and GAT-3 immunofluorescence in postmortem thalamic tissue (C) and perilesional cortex (D) from human subjects with a history of ischemic stroke or TBI, and age-matched control subjects. Images are representative of three control subjects, three subjects with stroke, and four subjects with TBI. Yellow boxes: regions magnified below. Summary of all data shown in fig. S11 and table S2.

thalamocortical rhythms—gain of function in pathological rhythms and loss of function in adaptive rhythms—as had been suggested by previous studies (*10*) but not yet demonstrated directly.

How might thalamic reactive astrocytes drive maladaptive circuit function? In the mouse model of thalamic astrogliosis, reactive astrocytes down-regulated the GAT-3 GABA transporter, leading to increased I_{TONIC} in thalamocortical neurons, resulting in increased neuronal excitability, and increased intrathalamic microcircuit excitability (fig. S12). Enhancing GAT-3 in mouse thalamic astrocytes prevented astrogliosis-induced neuronal hyperexcitability and restored cortical sigma and gamma power, supporting the conclusion that the maladaptive outcomes were driven by reactive astrocytes. As in our mouse model of thalamic astrogliosis, GAT-3 was also decreased in regions of thalamic reactive astrocytes in mouse models of cortical stroke and TBI. The identification of *SLC6A11*—encoding GAT-3—as a risk gene for epilepsy in humans (*66*) and the data showing that pharmacological blockade of GAT-3 strengthens epileptiform oscillations in rats ex vivo (*67*) suggest a link between GAT-3 and brain hyperexcitability. We found that enhancing astrocytic GAT-3 unilaterally in the thalamus prevented the increased seizure risk in the mouse model of thalamic astrogliosis and reduced chemoconvulsant-induced seizure severity and mortality in a mouse model of cortical injury.

At the mechanistic level, our study suggests that enhancing GAT-3 could act through reducing excess I_{TONIC} in thalamocortical neurons. In these cells, I_{TONIC} is mediated by the δ-subunit–containing $GABA_AR$ (encoded by *Gabrd*). *GABRD* is a susceptibility locus for generalized epilepsies, and increased I_{TONIC} has been implicated in epilepsy (*46*, *48*). Astrocytic GAT-3 plays a key role in the regulation of extrasynaptic GABA in the thalamus (*52*), which contributes to I_{TONIC} in thalamocortical neurons. In support of our hypothesis, preventing the increase in I_{TONIC} via conditional *Gabrd* deletion in thalamocortical neurons also prevented astrogliosis-driven hyperexcitability.

In the perilesional cortex of rodents, phasic and tonic GABA currents may play opposing roles in the aftermath of stroke (*68*, *69*). I_{TONIC} has diverse region- and cell type–specific effects (*48*). Thus, selectively counteracting the maladaptive components is critical in promoting repair. Although we did not examine changes in I_{TONIC} in thalamocortical neurons in TBI mice, our finding that enhancing thalamic GAT-3 prevented PTZ-induced mortality in TBI mice supports the idea that targeting thalamic astrocytic GAT-3 may be a viable strategy to decrease seizure risk after cortical injury.

Astrocytic GAT-3 activity and modulation of neuronal I_{TONIC} should be evaluated as possible therapeutic targets in the context of neuroinflammation associated with increased seizure risk. Dysfunction of GATs and I_{TONIC} has been implicated in various disorders associated with both chronic neuroinflammation and increased seizure risk, such as stroke (*69*) and Alzheimer's disease (*70*). Secondary and persistent astrogliosis of the thalamus is a predictor of long-term consequences of cortical lesions, such as epilepsy and cognitive impairment (*6*, *8*, *12*, *27*), and perturbations of cortical rhythms driven by thalamic astrogliosis (discussed above) phenocopy the changes observed in the aftermath of brain injuries. The secondarily damaged thalamus can be targeted to abort post-stroke epileptic seizures in rodents (*41*) and protect against chemoconvulsant-induced mortality in mice with TBI (discussed above). On the basis of our findings showing that GAT-3 loss of function is a hallmark of thalamic astrogliosis, and that increasing GAT-3 specifically in thalamic astrocytes is beneficial in multiple mouse models, we propose that GAT-3 loss of function is a node of failed homeostatic plasticity and a key component of reactive astrocyte dysfunction, which enables the far-reaching consequences of thalamic astrogliosis. In the sclerotic hippocampus, loss of GAT-1 is accompanied by an up-regulation in GAT-3, suggesting a compensatory homeostatic mechanism (*71*, *72*). However, in the setting of thalamic inflammation, loss of GAT-3 was not associated with transcriptional up-regulation of GAT-1. In the thalamus of humans and mice, *Slc6a11* (encoding GAT-3) is almost exclusively expressed in astrocytes (*56*, *57*), whereas *Slc6a1* (encoding GAT-1) is expressed similarly across astrocytes and neurons. Therefore, we speculate

that loss of GAT-3 in thalamic astrocytes might be particularly detrimental because of a homeostatic failure to compensate for lost function. We propose that enhancing GAT-3 in reactive astrocytes might promote brain resilience to injuries.

The mouse model of thalamic astrogliosis allows us to dissect the role of thalamic astrogliosis bypassing cortical injuries, but it has several limitations. First, a single experimental manipulation of astrocytes cannot fully phenocopy the molecular and functional features of reactive astrocytes. Nevertheless, our analyses highlight some features of astrogliosis conserved across experimental conditions—including somatic hypertrophy and reduction in process branching (*32*) and differential expression of canonical reactivity genes (*31*, *33*). Second, we did not investigate other elements of the neuroinflammatory cascade—such as the secondary activation of microglia—and therefore do not exclude their possible influence on circuit dysfunction after cortical lesions. Third, we did not investigate the extent to which astrogliosis-induced changes in cortical sigma and gamma power directly relate to disease-relevant cognitive or behavioral impairments. The absence of major abnormalities in mice with thalamic astrogliosis in standard behavioral assays relying on distributed brain circuits does not preclude other thalamocortical circuit–specific changes such as somatosensation or attention. Fourth, only male mice were included in our study. Given that the link between I_{TONIC} and neuronal excitability is ovarian cycle dependent (*73*), further investigations are needed to determine the relevance of our findings in female mice. Another limitation of this study was the limited sample size for postmortem thalamic human tissue, which excluded reliable statistical analysis of immunofluorescence data. We hope that our study will encourage inclusion of the thalamus in standard resection protocols of human postmortem brain tissue. In addition, because some data included in our study were obtained from patients with a history of epilepsy before and/or after injury, we cannot conclusively demonstrate that the changes in GFAP or GAT-3 were solely due to injury rather than recurrent seizures. Last, although we present evidence of thalamic GAT-3 perturbation across various model systems and proof of concept that thalamic GAT-3 can be targeted to prevent seizure risk in mice, further work in preclinical models of cortical injury is needed to understand whether GAT-3 can be safely targeted to ameliorate disease-relevant cellular and circuit pathologies such as spontaneous seizures without compromising the adaptive aspects of neuroinflammation.

MATERIALS AND METHODS

Study design

The main objective of this study was to investigate whether thalamic astrogliosis acts as a node of vulnerability after brain injuries, and if so, whether it represents a potential disease-modifying target. We developed a mouse model of unilateral thalamic astrogliosis using intrathalamic delivery of a viral construct previously shown to selectively induce reactive astrocytes in the hippocampus (*35*), used established mouse models of cortical injury (photothrombotic stroke and controlled cortical impact), and determined the potential restorative effects of counteracting GAT-3 loss using a viral construct to unilaterally enhance GAT-3 expression (*54*) in thalamic astrocytes. Transduction of reactive astrocytes was validated using established transcriptomic, morphological, and immunohistochemical markers (*28*) using a combination of transgenic reporter mice, FACS, bulk RNA sequencing (RNA-seq), and microscopy. Cellular excitability and synaptic function were assessed ex vivo with whole-cell current- and voltage-clamp recordings in thalamic neurons, and exclusion criteria are detailed below. Microcircuit excitability was assessed with extracellular recordings in ex vivo thalamic slices. In vivo brain excitability and cortical states were assessed with pharmacological seizure assays and ECoG recordings. Dysregulation of GAT-3 was assessed using a combination of immunohistochemistry, quantitative polymerase chain reaction (qPCR), bulk RNA-seq, and spatial transcriptomics in mice with thalamic astrogliosis and cortical injury. To assess relevance to human disease, immunohistochemical markers of astrogliosis and GAT-3 were assessed in postmortem thalamic tissue obtained from human subjects with a history of cortical injuries.

All mouse experiments were performed in adult, male, and age-matched mice with similar numbers randomly assigned to different experimental groups. Mice with thalamic astrogliosis were compared to mice injected unilaterally with sterile saline. Mice with cortical injury were compared to data from mice that received identical surgical procedures but no illumination of the light-sensitive dye (stroke) or impact (TBI). All procedures were approved by the ethics committees at the University of California San Francisco, Gladstone Institutes, and Amsterdam UMC. Sample sizes were based on similar previously published work (*10*, *12*, *43*, *74*) and are provided in figure legends. Data collection and analyses were performed blinded. Raw data are reported as a separate Excel document in data file S1.

Mice

All protocols were approved by the Institutional Animal Care and Use Committee at the University of California, San Francisco and Gladstone Institutes. Precautions were taken to minimize stress and the number of animals used in each set of experiments. Mice were separately housed after surgical implants.

Viral injections

Stereotaxic viral injections were carried out as previously described (*43*, *44*). Briefly, mice were anesthetized with 2 to 5% isoflurane. AAV constructs were delivered into the VB nucleus of the thalamus using the following coordinates: 1.65 mm posterior to bregma, 1.5 lateral relative to midline, and 3.3 to 3.5 mm ventral to the cortical surface. For all injections, the MicroSyringe Pump Controller (Micro4, WPI), NanoFil syringes (10 μl, WPI), and 33-g beveled NanoFil needles (NF33BV-2, WPI) were used. Viral constructs were infused at a rate of 100 to 200 nl/min, with a 5- to 10-min pause before withdrawing the needle. All viral injections were performed unilaterally. Experiments were performed at least 3 weeks after viral injections. Astrogliosis was induced with a high-titer injection of AAV2/5-Gfa104-PI.eGFP.WPRE.bGH (AAV2/5-Gfa104-eGFP), which transduces astrocytes with enhanced eGFP expression driven by a *Gfap* promoter (Addgene, no. 100896-AAV5; previously available through Penn Vector Core, catalog no. AV-5-PV2380) (*35*). Mice received unilateral injections of 750 nl of AAV2/5-Gfa104-eGFP or saline in control conditions (0.9% sodium chloride, Hospira). The titer of the construct, across various lots and experiments, was validated by Penn Vector Core using qPCR and droplet digital PCR and fell into the range of 0.85 to 1.7×10^{10} genome copies (g.c.) per injection. For low-titer control experiments, we delivered 1.4×10^{7} g.c. per injection. Previous work demonstrated that this titer does not induce astrogliosis (*35*). In describing the results of this study, we use "Control" to refer to mice in which we

performed intrathalamic injection of saline, and we use "Thalamic Astrogliosis" to refer to mice in which we performed intrathalamic injections of AAV2/5-Gfa104-eGFP unless specified otherwise. To selectively delete the delta subunit in *Gabrd*$^{Fl/Fl}$ mice, 600 nl of AAV-CaMKIIα-mCherry-Cre (UNC Vector Core) was used in combination with 750 nl of either AAV2/5-Gfa104-eGFP or saline. AAV2/5-GfaABC$_1$D-GAT3-HA-mCherry (generated by B.S.K. and X.Y.) was used to selectively enhance expression of GAT-3 in astrocytes. A total of 600 nl of AAV-GAT3 was delivered in combination with 750 nl of either AAV2/5-Gfa104-eGFP or saline.

Patch-clamp electrophysiology in thalamic slices

Recordings were performed as previously described (*12*, *43*, *75*). Thalamocortical neurons in the VB thalamus, and neurons in the nRT, were visually identified by differential contrast optics with an Olympus microscope (60× objective; numerical aperture, 1.1; working distance 1.5 mm; SKU 1-U2M592). Recording electrodes made of borosilicate glass (Sutter Instruments) had a resistance of 2.5 to 4 megohms when filled with intracellular solution. Access resistance was monitored in all the recordings, and cells were included for analysis only if the access resistance was <25 megohms.

To record intrinsic membrane properties and bursting properties in current-clamp mode, and spontaneous excitatory postsynaptic currents in voltage-clamp mode, an internal solution containing 120 mM potassium gluconate, 11 mM KCl, 1 mM $MgCl_2$, 1 mM $CaCl_2$, 10 mM Hepes, and 1 mM EGTA, pH adjusted to 7.4 with KOH (290 mOsm/kg), was used; these recordings were performed in the presence of picrotoxin (50 μM; Sigma-Aldrich, no. P1675) in the artificial cerebrospinal fluid (aCSF). The potentials were corrected offline for −15 mV liquid junction potential.

To record spontaneous inhibitory postsynaptic currents, an internal solution containing 135 mM CsCl, 10 mM Hepes, 10 mM EGTA, 2 mM $MgCl_2{\cdot}6H_2O$, and 5 mM QX-314, pH adjusted to 7.3 with CsOH (290 mOsm/kg), was used. Recordings were performed in the presence of kynurenic acid (2 mM, Sigma-Aldrich, no. K3375) in aCSF. To record tonic $GABA_AR$-mediated currents, an internal solution containing 130 mM CsCl, 2 mM $MgCl_2$, 4 mM Mg-adenosine triphosphate, 0.3 mM Na-guanosine triphosphate, 10 mM Na-Hepes, and 0.1 mM EGTA, pH adjusted to 7.3 with CsOH (290 mOsm/kg), was used (*45*).

Recordings were performed in the presence of kynurenic acid (2 mM) in aCSF, which was kept at 30°± 1°C. To obtain tonic GABA measurements, a bath of 50 μM gabazine (GBZ; Sigma-Aldrich, no. SR-95531) prepared in dimethyl sulfoxide (Sigma-Aldrich, no. D8418) was applied. After GBZ application, slices were recorded for at least 10 min. Tonic current was defined as the shift in holding current due to GBZ bath application and marked by the stopping of phasic inhibitory postsynaptic currents. Average currents were obtained for at least 2 min pre- and post-stabilization of the shift in holding current. Currents were subtracted using Clampfit 10.5 (Molecular Devices, SCR_011323). Currents are presented without normalizing to cell capacitance, as capacitance did not differ between groups (table S3).

In vivo ECoG data acquisition

To control for circadian rhythms, animals were housed using a regular light/dark cycle, and recordings were performed between 7:00 a.m. and 7:00 p.m. Before acquisition of multisite ECoG recordings (Figs. 4 and 5 and fig. S6), mice were allowed to recover for at least 1 week. ECoG signals were recorded using RZ5 via Synapse software (Tucker Davis Technologies) and sampled at 1221 Hz. Animals were continuously monitored during recordings using a video camera that was synchronized to the signal acquisition via RZ5 (*43*).

Chronic, continuous ECoG recordings (Fig. 6 and table S9) were acquired using wireless telemetry devices (PhysioTel HD-X02 implants, Data Sciences International) and sampled at 500 Hz via Ponemah software (DSI). Recordings (24 hours a day, 7 days a week) were performed for 1-week periods (168 hours) at the following time points: 1, 3, 5, and 7 weeks after thalamic astrogliosis (Fig. 6C), and 7 weeks after thalamic astrogliosis with GAT-3 enhancement (Fig. 6D). Acquisition started immediately after implantation, as the wireless devices allow mice to remain in their home cages.

Quantification and statistical analysis

In vivo ECoG

Detection of epileptiform discharges. To quantify the number of epileptiform discharges, induced by PTZ, we used a custom MATLAB script, which enabled the detection of synchronous discharges with amplitude three times the baseline signal noise and required user input to reject or accept events. Quantification was performed for the somatosensory cortex ipsilateral to thalamic astrogliosis and compared with a Mann-Whitney *U* test. This detection method was validated against manual quantification of epileptiform discharges from the raw ECoG and simultaneously acquired video recordings of mice. A subset of mice presented in Fig. 4D underwent the PTZ seizure assay again at 4 and/or 7 months to determine the chronic effects of astrogliosis (presented in fig. S6).

Kainic acid seizure detection. Seizures on EEG traces were identified on the basis of high-frequency, synchronous discharges with amplitude three times the baseline signal noise, using Spike2 software. Detection was cross-validated with behavioral signs of seizures from simultaneously acquired video recordings of mice.

ECoG spectral analysis. For chronic, continuous ECoG recordings, spectral analysis was performed in MATLAB. Absolute power of individual frequency bands was calculated using the band power function in MATLAB. Total band power was calculated between 1 and 75 Hz to avoid edge effects of the wireless device bandwidth (0.5 to 80 Hz). For weeks 1, 5, and 7, we obtained 168 1-hour bins; for week 3, we obtained 152 1-hour bins. Total band power was calculated between 1 and 75 Hz to avoid edge effects of the wireless device bandwidth (0.5 to 80 Hz). To analyze spectral features at week 7 (the most chronic time point tested), we calculated the absolute power of individual frequency bands for 12-hour bins corresponding to the light and dark cycle. To investigate spectral features of the somatosensory cortex (S1) functionally connected to the site of thalamic astrogliosis, we performed paired *t* tests of frequency bands obtained from ipsilateral and contralateral S1. All statistical comparisons are reported in table S9.

Statistical analysis

All numerical values are given as means, and error bars are SEM unless stated otherwise. For comparison between two groups, the nonparametric Mann-Whitney *U* test was performed. For comparisons between multiple groups, a one- or two-way analysis of variance (ANOVA; ordinary or repeated measures) was performed, in addition to post hoc comparisons with corrections for multiple comparisons (detailed in figure legends). When parametric tests were used, results of the Shapiro-Wilk normality test are provided. The threshold for statistical significance was set to $\alpha = 0.05$ unless

specified otherwise. Each *n* represents an independent biological sample unless specified otherwise in figure legends. Data analysis was performed with MATLAB, GraphPad Prism 7, OriginPro, SigmaPlot, and SPSS.

SUPPLEMENTARY MATERIALS

www.science.org/doi/10.1126/scitranslmed.abj4310
Materials and Methods
Figs. S1 to S12
Tables S1 to S10
Data files S1 and S2
MDAR Reproducibility Checklist

View/request a protocol for this paper from *Bio-protocol*.

REFERENCES AND NOTES

1. M. V. Russo, D. B. McGavern, Inflammatory neuroprotection following traumatic brain injury. *Science* **353**, 783–785 (2016).
2. D. W. Simon, M. J. McGeachy, H. Baylr, R. S. B. Clark, D. J. Loane, P. M. Kochanek, The far-reaching scope of neuroinflammation after traumatic brain injury. *Nat. Rev. Neurol.* **13**, 171–191 (2017).
3. A. Vezzani, S. Balosso, T. Ravizza, Neuroinflammatory pathways as treatment targets and biomarkers in epilepsy. *Nat. Rev. Neurol.* **15**, 459–472 (2019).
4. S. X. Shi, K. Shi, Q. Liu, Brain injury instructs bone marrow cellular lineage destination to reduce neuroinflammation. *Sci. Transl. Med.* **13**, eabc7029 (2021).
5. I. L. Llorente, Y. Xie, J. A. Mazzitelli, E. A. Hatanaka, J. Cinkornpumin, D. R. Miller, Y. Lin, W. E. Lowry, S. T. Carmichael, Patient-derived glial enriched progenitors repair functional deficits due to white matter stroke and vascular dementia in rodents. *Sci. Transl. Med.* **13**, eaaz6747 (2021).
6. E. J. Grossman, M. Inglese, The role of thalamic damage in mild traumatic brain injury. *J. Neurotrauma* **33**, 163–167 (2016).
7. G. Scott, P. J. Hellyer, A. F. Ramlackhansingh, D. J. Brooks, P. M. Matthews, D. J. Sharp, Thalamic inflammation after brain trauma is associated with thalamo-cortical white matter damage. *J. Neuroinflammation* **12**, 224 (2015).
8. A. F. Ramlackhansingh, D. J. Brooks, R. J. Greenwood, S. K. Bose, F. E. Turkheimer, K. M. Kinnunen, S. Gentleman, R. A. Heckemann, K. Gunanayagam, G. Gelosa, D. J. Sharp, Inflammation after trauma: Microglial activation and traumatic brain injury. *Ann. Neurol.* **70**, 374–383 (2011).
9. W. L. Maxwell, M. A. MacKinnon, D. H. Smith, T. K. McIntosh, D. I. Graham, Thalamic nuclei after human blunt head injury. *J. Neuropathol. Exp. Neurol.* **65**, 478–488 (2006).
10. S. S. Holden, F. C. Grandi, O. Aboubakr, B. Higashikubo, F. S. Cho, A. H. Chang, A. O. Forero, A. R. Morningstar, V. Mathur, L. J. Kuhn, P. Suri, S. Sankaranarayanan, Y. Andrews-Zwilling, A. J. Tenner, A. Luthi, E. Aronica, M. R. Corces, T. Yednock, J. T. Paz, Complement factor C1q mediates sleep spindle loss and epileptic spikes after mild brain injury. *Science* **373**, eabj2685 (2021).
11. A. Hazra, C. Macolino, M. B. Elliott, J. Chin, Delayed thalamic astrocytosis and disrupted sleep-wake patterns in a preclinical model of traumatic brain injury. *J. Neurosci. Res.* **92**, 1434–1445 (2014).
12. J. T. Paz, C. A. Christian, I. Parada, D. A. Prince, J. R. Huguenard, Focal cortical infarcts alter intrinsic excitability and synaptic excitation in the reticular thalamic nucleus. *J. Neurosci.* **30**, 5465–5479 (2010).
13. Z. Cao, S. S. Harvey, T. M. Bliss, M. Y. Cheng, G. K. Steinberg, Inflammatory responses in the secondary thalamic injury after cortical ischemic stroke. *Front. Neurol.* **11**, 236 (2020).
14. S. Pappata, M. Levasseur, R. N. Gunn, R. Myers, C. Crouzel, A. Syrota, T. Jones, G. W. Kreutzberg, R. B. Banati, Thalamic microglial activation in ischemic stroke detected in vivo by PET and [11C]PK11195. *Neurology* **55**, 1052–1054 (2000).
15. G. C. Beattie, C. A. Glaser, H. Sheriff, S. Messenger, C. P. Preas, M. Shahkarami, A. Venkatesan, Encephalitis with thalamic and basal ganglia abnormalities: Etiologies, neuroimaging, and potential role of respiratory viruses. *Clin. Infect. Dis.* **56**, 825–832 (2013).
16. J. C. Guth, S. A. Futterer, T. A. Hijaz, E. M. Liotta, N. F. Rosenberg, A. M. Naidech, M. B. Maas, Pearls & Oy-sters: Bilateral thalamic involvement in West Nile virus encephalitis. *Neurology* **83**, e16–e17 (2014).
17. D. Abel, M. Y. Shen, Z. Abid, C. Hennigan, A. Boneparth, E. H. Miller, A. C. Uhlemann, D. K. McBrian, K. Thakur, W. Silver, J. M. Bain, Encephalopathy and bilateral thalamic lesions in a child with MIS-C associated with COVID-19. *Neurology* **95**, 745–748 (2020).
18. N. Poyiadji, G. Shahin, D. Noujaim, M. Stone, S. Patel, B. Griffith, COVID-19-associated acute hemorrhagic necrotizing encephalopathy: Imaging features. *Radiology* **296**, E119–E120 (2020).
19. J. Zheng, L. Y. R. Wong, K. Li, A. K. Verma, M. Ortiz, C. Wohlford-Lenane, M. R. Leidinger, C. M. Knudson, D. K. Meyerholz, P. B. McCray, S. Perlman, COVID-19 treatments and pathogenesis including anosmia in K18-hACE2 mice. *Nature* **589**, 603–607 (2021).
20. D. Jeanmonod, M. Magnin, A. Morel, Low-threshold calcium spike bursts in the human thalamus: Common physiopathology for sensory, motor and limbic positive symptoms. *Brain* **119**, 363–375 (1996).
21. M. Steriade, D. A. McCormick, T. J. Sejnowski, Thalamocortical oscillations in the sleeping and aroused brain. *Science* **262**, 679–685 (1993).
22. M. Steriade, D. Contreras, F. Amzica, I. Timofeev, Synchronization of fast (30-40 Hz) spontaneous oscillations in intrathalamic and thalamocortical networks. *J. Neurosci.* **16**, 2788–2808 (1996).
23. V. Crunelli, S. W. Hughes, The slow (1 Hz) rhythm of non-REM sleep: A dialogue between three cardinal oscillators. *Nat. Neurosci.* **13**, 9–17 (2010).
24. P. M. Fogerson, J. R. Huguenard, Tapping the brakes: Cellular and synaptic mechanisms that regulate thalamic oscillations. *Neuron* **92**, 687–704 (2016).
25. E. G. Jones, The thalamic matrix and thalamocortical synchrony. *Trends Neurosci.* **24**, 595–601 (2001).
26. J. T. Paz, J. R. Huguenard, Microcircuits and their interactions in epilepsy: Is the focus out of focus? *Nat. Neurosci.* **18**, 351–359 (2015).
27. E. J. Grossman, Y. Ge, J. H. Jensen, J. S. Babb, L. Miles, J. Reaume, J. M. Silver, R. I. Grossman, M. Inglese, Thalamus and cognitive impairment in mild traumatic brain injury: A diffusional kurtosis imaging study. *J. Neurotrauma* **29**, 2318–2327 (2012).
28. C. Escartin, E. Galea, A. Lakatos, J. P. O'Callaghan, G. C. Petzold, A. Serrano-Pozo, C. Steinhäuser, A. Volterra, G. Carmignoto, A. Agarwal, N. J. Allen, A. Araque, L. Barbeito, A. Barzilai, D. E. Bergles, G. Bonvento, A. M. Butt, W.-T. Chen, M. Cohen-Salmon, C. Cunningham, B. Deneen, B. De Strooper, B. Díaz-Castro, C. Farina, M. Freeman, V. Gallo, J. E. Goldman, S. A. Goldman, M. Götz, A. Gutiérrez, P. G. Haydon, D. H. Heiland, E. M. Hol, M. G. Holt, M. Iino, K. V. Kastanenka, H. Kettenmann, B. S. Khakh, S. Koizumi, C. J. Lee, S. A. Liddelow, B. A. MacVicar, P. Magistretti, A. Messing, A. Mishra, A. V. Molofsky, K. K. Murai, C. M. Norris, S. Okada, S. H. R. Oliet, J. F. Oliveira, A. Panatier, V. Parpura, M. Pekna, M. Pekny, L. Pellerin, G. Perea, B. G. Pérez-Nievas, F. W. Pfrieger, K. E. Poskanzer, F. J. Quintana, R. M. Ransohoff, M. Riquelme-Perez, S. Robel, C. R. Rose, J. D. Rothstein, N. Rouach, D. H. Rowitch, A. Semyanov, S. Sirko, H. Sontheimer, R. A. Swanson, J. Vitorica, I.-B. Wanner, L. B. Wood, J. Wu, B. Zheng, E. R. Zimmer, R. Zorec, M. V. Sofroniew, A. Verkhratsky, Reactive astrocyte nomenclature, definitions, and future directions. *Nat. Neurosci.* **24**, 312–325 (2021).
29. J. E. Burda, M. V. Sofroniew, Reactive gliosis and the multicellular response to CNS damage and disease. *Neuron* **81**, 229–248 (2014).
30. E. Colombo, C. Farina, Astrocytes: Key regulators of neuroinflammation. *Trends Immunol.* **37**, 608–620 (2016).
31. S. A. Liddelow, K. A. Guttenplan, L. E. Clarke, F. C. Bennett, C. J. Bohlen, L. Schirmer, M. L. Bennett, A. E. Münch, W.-S. Chung, T. C. Peterson, D. K. Wilton, A. Frouin, B. A. Napier, N. Panicker, M. Kumar, M. S. Buckwalter, D. H. Rowitch, V. L. Dawson, T. M. Dawson, B. Stevens, B. A. Barres, Neurotoxic reactive astrocytes are induced by activated microglia. *Nature* **541**, 481–487 (2017).
32. D. Sun, T. C. Jakobs, Structural remodeling of astrocytes in the injured CNS. *Neuroscientist* **18**, 567–588 (2012).
33. J. Zamanian, L. Xu, L. Foo, N. Nouri, L. Zhou, R. Giffard, B. Barres, Genomic analysis of reactive astrogliosis. *J. Neurosci.* **32**, 6391–6410 (2012).
34. D. Necula, F. S. Cho, A. He, J. T. Paz, Secondary thalamic neuroinflammation after focal cortical stroke and traumatic injury mirrors corticothalamic functional connectivity. *J. Comp. Neurol.* **530**, 998–1019 (2022).
35. P. I. Ortinski, J. Dong, A. Mungenast, C. Yue, H. Takano, D. J. Watson, P. G. Haydon, D. A. Coulter, Selective induction of astrocytic gliosis generates deficits in neuronal inhibition. *Nat. Neurosci.* **13**, 584–591 (2010).
36. L. Morel, H. Higashimori, M. Tolman, Y. Yang, VGluT1+ neuronal glutamatergic signaling regulates postnatal developmental maturation of cortical protoplasmic astroglia. *J. Neurosci.* **34**, 10950–10962 (2014).
37. T. A. Ferreira, A. V. Blackman, J. Oyrer, S. Jayabal, A. J. Chung, A. J. Watt, P. J. Sjöström, D. J. Van Meyel, Neuronal morphometry directly from bitmap images. *Nat. Methods* **11**, 982–984 (2014).
38. D. C. Patel, B. P. Tewari, L. Chaunsali, H. Sontheimer, Neuron–glia interactions in the pathophysiology of epilepsy. *Nat. Rev. Neurosci.* **20**, 282–297 (2019).
39. M. M. Huntsman, D. M. Porcello, G. E. Homanics, T. M. DeLorey, J. R. Huguenard, Reciprocal inhibitory connections and network synchrony in the mammalian thalamus. *Science* **283**, 541–543 (1999).
40. L. Cueni, M. Canepari, R. Luján, Y. Emmenegger, M. Watanabe, C. T. Bond, P. Franken, J. P. Adelman, A. Lüthi, T-type Ca 2+ channels, SK2 channels and SERCAs gate sleep-related oscillations in thalamic dendrites. *Nat. Neurosci.* **11**, 683–692 (2008).
41. J. T. Paz, T. J. Davidson, E. S. Frechette, B. Delord, I. Parada, K. Peng, K. Deisseroth, J. R. Huguenard, Closed-loop optogenetic control of thalamus as a tool for interrupting seizures after cortical injury. *Nat. Neurosci.* **16**, 64–70 (2013).

42. F. S. Cho, A. Clemente, S. Holden, J. T. Paz, in *Models of Seizures and Epilepsy*, A. Pitkänen, P. Buckmaster, A. S. Galanopoulou, S. L. Moshé, Eds. (Academic Press, ed. 2, 2017), pp. 273–284.
43. S. Ritter-Makinson, A. Clemente-Perez, B. Higashikubo, F. S. Cho, S. S. Holden, E. Bennett, A. Chkaidze, O. H. J. E. Rooda, M. C. Cornet, F. E. Hoebeek, K. Yamakawa, M. R. Cilio, B. Delord, J. T. Paz, Augmented reticular thalamic bursting and seizures in Scn1a-dravet syndrome. *Cell Rep.* **26**, 54–64.e6 (2019).
44. J. M. Sorokin, T. J. Davidson, E. Frechette, A. M. Abramian, K. Deisseroth, J. R. Huguenard, J. T. Paz, Bidirectional control of generalized epilepsy networks via rapid real-time switching of firing mode. *Neuron* **93**, 194–210 (2017).
45. D. W. Cope, S. W. Hughes, V. Crunelli, GABAA receptor-mediated tonic inhibition in thalamic neurons. *J. Neurosci.* **25**, 11553–11563 (2005).
46. D. W. Cope, G. Di Giovanni, S. J. Fyson, G. Orbán, A. C. Errington, M. L. Lőrincz, T. M. Gould, D. A. Carter, V. Crunelli, Enhanced tonic GABAA inhibition in typical absence epilepsy. *Nat. Med.* **15**, 1392–1398 (2009).
47. D. A. Coulter, J. R. Huguenard, D. A. Prince, Calcium currents in rat thalamocortical relay neurones: Kinetic properties of the transient, low-threshold current. *J. Physiol.* **414**, 587–604 (1989).
48. V. Lee, J. Maguire, The impact of tonic $GABA_A$ receptor-mediated inhibition on neuronal excitability varies across brain region and cell type. *Front. Neural Circuits* **8**, 3 (2014).
49. A. Agmon, L. T. Yang, D. K. O'Dowd, E. G. Jones, Organized growth of thalamocortical axons from the deep tier of terminations into layer IV of developing mouse barrel cortex. *J. Neurosci.* **13**, 5365–5382 (1993).
50. J. L. Wagnon, M. J. Korn, R. Parent, T. A. Tarpey, J. M. Jones, M. F. Hammer, G. G. Murphy, J. M. Parent, M. H. Meisler, Convulsive seizures and SUDEP in a mouse model of SCN8A epileptic encephalopathy. *Hum. Mol. Genet.* **24**, 506–515 (2015).
51. V. Lee, J. Maguire, Impact of inhibitory constraint of interneurons on neuronal excitability. *J. Neurophysiol.* **110**, 2520–2535 (2013).
52. M. P. Beenhakker, J. R. Huguenard, Astrocytes as gatekeepers of GABAB receptor function. *J. Neurosci.* **30**, 15262–15276 (2010).
53. T. Pirttimaki, H. R. Parri, V. Crunelli, Astrocytic GABA transporter GAT-1 dysfunction in experimental absence seizures. *J. Physiol.* **591**, 823–833 (2013).
54. X. Yu, A. M. W. Taylor, J. Nagai, P. Golshani, C. J. Evans, G. Coppola, B. S. Khakh, Reducing astrocyte calcium signaling in vivo alters striatal microcircuits and causes repetitive behavior. *Neuron* **99**, 1170–1187.e9 (2018).
55. K. W. Kelley, H. Nakao-Inoue, A. V. Molofsky, M. C. Oldham, Variation among intact tissue samples reveals the core transcriptional features of human CNS cell classes. *Nat. Neurosci.* **21**, 1171–1184 (2018).
56. S. De Biasi, L. Vitellaro-Zuccarello, N. C. Brecha, Immunoreactivity for the GABA transporter-1 and GABA transporter-3 is restricted to astrocytes in the rat thalamus. A light and electron- microscopic immunolocalization. *Neuroscience* **83**, 815–828 (1998).
57. L. Vitellaro-Zuccarello, N. Calvaresi, S. De Biasi, Expression of GABA transporters, GAT-1 and GAT-3, in the cerebral cortex and thalamus of the rat during postnatal development. *Cell Tissue Res.* **313**, 245–257 (2003).
58. S. Robel, S. C. Buckingham, J. L. Boni, S. L. Campbell, N. C. Danbolt, T. Riedemann, B. Sutor, H. Sontheimer, Reactive astrogliosis causes the development of spontaneous seizures. *J. Neurosci.* **35**, 3330–3345 (2015).
59. S. Robel, H. Sontheimer, Glia as drivers of abnormal neuronal activity. *Nat. Neurosci.* **19**, 28–33 (2016).
60. M. Maroso, S. Balosso, T. Ravizza, J. Liu, E. Aronica, A. M. Iyer, C. Rossetti, M. Molteni, M. Casalgrandi, A. A. Manfredi, M. E. Bianchi, A. Vezzani, Toll-like receptor 4 and high-mobility group box-1 are involved in ictogenesis and can be targeted to reduce seizures. *Nat. Med.* **16**, 413–419 (2010).
61. V. V. Senatorov, A. R. Friedman, D. Z. Milikovsky, J. Ofer, R. Saar-Ashkenazy, A. Charbash, N. Jahan, G. Chin, E. Mihaly, J. M. Lin, H. J. Ramsay, A. Moghbel, M. K. Preininger, C. R. Eddings, H. V. Harrison, R. Patel, Y. Shen, H. Ghanim, H. Sheng, R. Veksler, P. H. Sudmant, A. Becker, B. Hart, M. A. Rogawski, A. Dillin, A. Friedman, D. Kaufer, Blood-brain barrier dysfunction in aging induces hyper-activation of TGF-beta signaling and chronic yet reversible neural dysfunction. *Sci. Transl. Med.* **11**, eaaw8283 (2019).
62. C. Steinhäuser, G. Seifert, in *Jasper's Basic Mechanisms of the Epilepsies*, J. L. Noebels, M. Avoli, M. A. Rogawski, R. W. Olsen, A. V. Delgado-Escueta Eds. (National Center for Biotechnology Information (US), ed. 4, 2012).
63. P. Klein, R. Dingledine, E. Aronica, C. Bernard, I. Blümcke, D. Boison, M. J. Brodie, A. R. Brooks-Kayal, J. Engel, P. A. Forcelli, L. J. Hirsch, R. M. Kaminski, H. Klitgaard, K. Kobow, D. H. Lowenstein, P. L. Pearl, A. Pitkänen, N. Puhakka, M. A. Rogawski, D. Schmidt, M. Sillanpää, R. S. Sloviter, C. Steinhäuser, A. Vezzani, M. C. Walker, W. Löscher, Commonalities in epileptogenic processes from different acute brain insults: Do they translate? *Epilepsia* **59**, 37–66 (2018).
64. P. Andrade, J. Nissinen, A. Pitkänen, Generalized seizures after experimental traumatic brain injury occur at the transition from slow-wave to rapid eye movement sleep. *J. Neurotrauma* **34**, 1482–1487 (2017).
65. M. C. Ouellet, S. Beaulieu-Bonneau, C. M. Morin, Sleep-wake disturbances after traumatic brain injury. *Lancet Neurol.* **14**, 746–757 (2015).
66. O. E. M. G. Schijns, J. Bisschop, K. Rijkers, J. Dings, S. Vanherle, P. Lindsey, H. J. M. Smeets, G. Hoogland, GAT-1 (rs2697153) and GAT-3 (rs2272400) polymorphisms are associated with febrile seizures and temporal lobe epilepsy. *Epileptic Disord.* **22**, 176–182 (2020).
67. A. C. Lu, C. K. Lee, M. Kleiman-Weiner, B. Truong, M. Wang, J. R. Huguenard, M. P. Beenhakker, Nonlinearities between inhibition and t-type calcium channel activity bidirectionally regulate thalamic oscillations. *eLife* **9**, e59548 (2020).
68. T. Hiu, Z. Farzampour, J. T. Paz, E. H. J. Wang, C. Badgely, A. Olson, K. D. Micheva, G. Wang, R. Lemmens, K. V. Tran, Y. Nishiyama, X. Liang, S. A. Hamilton, N. O'Rourke, S. J. Smith, J. R. Huguenard, T. M. Bliss, G. K. Steinberg, Enhanced phasic GABA inhibition during the repair phase of stroke: A novel therapeutic target. *Brain* **139**, 468–480 (2016).
69. A. N. Clarkson, B. S. Huang, S. E. Macisaac, I. Mody, S. T. Carmichael, Reducing excessive GABA-mediated tonic inhibition promotes functional recovery after stroke. *Nature* **468**, 305–309 (2010).
70. S. Jo, O. Yarishkin, Y. J. Hwang, Y. E. Chun, M. Park, D. H. Woo, J. Y. Bae, T. Kim, J. Lee, H. Chun, H. J. Park, D. Y. Lee, J. Hong, H. Y. Kim, S. J. Oh, S. J. Park, H. Lee, B. E. Yoon, Y. Kim, Y. Jeong, I. Shim, Y. C. Bae, J. Cho, N. W. Kowall, H. Ryu, E. Hwang, D. Kim, C. J. Lee, GABA from reactive astrocytes impairs memory in mouse models of Alzheimer's disease. *Nat. Med.* **20**, 886–896 (2014).
71. Z. Wu, Z. Guo, M. Gearing, G. Chen, Tonic inhibition in dentate gyrus impairs long-term potentiation and memory in an Alzhiemer's disease model. *Nat. Commun.* **5**, 4159 (2014).
72. T. S. Lee, L. P. Bjørnsen, C. Paz, J. H. Kim, S. S. Spencer, D. D. Spencer, T. Eid, N. C. Lanerolle, GAT1 and GAT3 expression are differently localized in the human epileptogenic hippocampus. *Acta Neuropathol.* **111**, 351–363 (2006).
73. J. L. Maguire, B. M. Stell, M. Rafizadeh, I. Mody, Ovarian cycle-linked changes in GABAA receptors mediating tonic inhibition alter seizure susceptibility and anxiety. *Nat. Neurosci.* **8**, 797–804 (2005).
74. I. D. Vainchtein, G. Chin, F. S. Cho, K. W. Kelley, J. G. Miller, E. C. Chien, S. A. Liddelow, P. T. Nguyen, H. Nakao-inoue, L. C. Dorman, O. Akil, S. Joshita, B. A. Barres, J. T. Paz, A. B. Molofsky, A. V. Molofsky, Astrocyte-derived interleukin-33 promotes microglial synapse engulfment and neural circuit development. *Science* **359**, 1269–1273 (2018).
75. J. T. Paz, A. S. Bryant, K. Peng, L. Fenno, O. Yizhar, W. N. Frankel, K. Deisseroth, J. R. Huguenard, A new mode of corticothalamic transmission revealed in the $Gria4^{-/-}$ model of absence epilepsy. *Nat. Neurosci.* **14**, 1167–1173 (2011).
76. K. B. J. Franklin, G. Paxinos, *The Mouse Brain in Stereotaxic Coordinates* (Elsevier Academic Press, ed. 3, 2007).
77. A. Schousboe, L. K. Bak, H. S. Waagepetersen, Astrocytic control of biosynthesis and turnover of the neurotransmitters glutamate and GABA. *Front. Endocrinol.* **4**, 102 (2013).
78. T. F. Galatro, I. R. Holtman, A. M. Lerario, I. D. Vainchtein, N. Brouwer, P. R. Sola, M. M. Veras, T. F. Pereira, R. E. P. Leite, T. Möller, P. D. Wes, M. C. Sogayar, J. D. Laman, W. den Dunnen, C. A. Pasqualucci, S. M. Oba-Shinjo, E. W. G. M. Boddeke, S. K. N. Marie, B. J. L. Eggen, Transcriptomic analysis of purified human cortical microglia reveals age-associated changes. *Nat. Neurosci.* **20**, 1162–1171 (2017).
79. J. D. Cahoy, B. Emery, A. Kaushal, L. C. Foo, J. L. Zamanian, K. S. Christopherson, Y. Xing, J. L. Lubischer, P. A. Krieg, S. A. Krupenko, W. J. Thompson, B. A. Barres, A transcriptome database for astrocytes, neurons, and oligodendrocytes: A new resource for understanding brain development and function. *J. Neurosci.* **28**, 264–278 (2008).
80. E. A. van Vliet, X. E. Ndode-Ekane, L. J. Lehto, J. A. Gorter, P. Andrade, E. Aronica, O. Gröhn, A. Pitkänen, Long-lasting blood-brain barrier dysfunction and neuroinflammation after traumatic brain injury. *Neurobiol. Dis.* **145**, 105080 (2020).
81. S. Pangratz-Fuehrer, W. Sieghart, U. Rudolph, I. Parada, J. R. Huguenard, Early postnatal switch in GABAA receptor α-subunits in the reticular thalamic nucleus. *J. Neurophysiol.* **115**, 1183–1195 (2016).
82. D. A. McCormick, H.-C. Pape, Properties of a hyperpolarization-activated cation current and its role in rhythmic oscillation in thalamic relay neurones. *J. Physiol.* **431**, 291–318 (1990).
83. M. A. Mirski, J. A. Ferrendelli, Anterior thalamic mediation of generalized pentylenetetrazol seizures. *Brain Res.* **399**, 212–223 (1986).
84. T. Bolkvadze, A. Pitkänen, Development of post-traumatic epilepsy after controlled cortical impact and lateral fluid-percussion-induced brain injury in the mouse. *J. Neurotrauma* **29**, 789–812 (2012).
85. E. D. Roberson, K. Scearce-Levie, J. J. Palop, F. Yan, I. H. Cheng, T. Wu, H. Gerstein, G. Q. Yu, L. Mucke, Reducing endogenous tau ameliorates amyloid ß-induced deficits in an Alzheimer's cisease mouse model. *Science* **316**, 750–754 (2007).
86. E. Manninen, K. Chary, N. Lapinlampi, P. Andrade, T. Paananen, A. Sierra, J. Tohka, O. Gröhn, A. Pitkänen, Acute thalamic damage as a prognostic biomarker for post-traumatic epileptogenesis. *Epilepsia* **62**, 1852–1864 (2021).
87. R. F. Hunt, S. W. Scheff, B. N. Smith, Posttraumatic epilepsy after controlled cortical impact injury in mice. *Exp. Neurol.* **215**, 243–252 (2009).

Acknowledgments: We thank J. Maguire for providing the *Gabrd*$^{Fl/Fl}$ mice; J. Huguenard and J. Sorokin for providing the custom MATLAB script for thalamic oscillation analysis; K. Kelley and M. Oldham for providing assistance in using published database of human transcriptomic data; I. Lew and H. Inoue for help with animal husbandry; N. Jahan for technical assistance; K. Claiborn and F. Chanut for providing critical editorial feedback on the manuscript; R. Thomas (Gladstone Bioinformatics Core) for consultation of statistical analyses; L. Mucke and M. Gill, and I. Lo and J. Sims (Gladstone Behavioral Core) for consultation on behavioral experiments; J. McGuire (Gladstone Genomics Core) for conducting the RNA sequencing library preparation and QCs for sequencing at the Center For Advanced Technology at UCSF; and the Gladstone Histology Core for technical advice. **Funding:** This work was supported by National Institute of Neurological Disorders and Stroke grants F31 NS111819 (to F.S.C.), R01 NS096369 (to J.T.P.), R01 NS121287 (to J.T.P.), R00 NS078118 (to J.T.P.), and R35 NS111583 (to B.S.K.); National Institute of Mental Health grants DP1 MH104069 (to B.S.K.), DP2 MH116507 (to A.V.M.), and R01 MH119349 (to A.V.M.); National Cancer Institute grant P30 CA082103 (to UCSF Laboratory for Cell Analysis); National Science Foundation grant 1144247 (to F.S.C.); UCSF Discovery Fellowship (to F.S.C.); Department of Defense grants EP150038 and EP190020 (to J.T.P.); Gladstone Institutes Animal Facility grant RR18928 (to J.T.P.); Pew Charitable Trusts (to A.V.M.); European Union Seventh Framework Programme EPITARGET grant 602102 (to E.A.v.V. and E.A.); European Union Horizon 2020 Research and Innovation Programme Marie Sklodowska-Curie grant 722053 (to E.A.); Dutch Epilepsy Foundation project 16-05 (to D.W.M.B. and E.A.); and European Union Horizon 2020 WIDESPREAD-05-2020-Twinning, EpiEpiNet grant agreement 952455 (to E.A. and E.A.v.V.). **Author contributions:** F.S.C. and J.T.P. conceived the project. F.S.C. performed stereotaxic viral injections, ECoG implants, in vivo recordings and analysis, ex vivo electrophysiological studies and analysis, immunohistochemistry, and all related data analysis and visualization. I.D.V. performed, analyzed, and interpreted FACS, bulk transcriptomics, and qPCR studies. I.D.V. and F.S.C. performed, analyzed, and interpreted astrocyte morphology study. D.W.M.B., J.J.A., E.A.v.V., and E.A. performed, analyzed, and interpreted immunolabeling of postmortem human tissue. B.S.K. and X.Y. generated the AAV2/5-GfaABC$_1$D-GAT3-HA-mCherry construct. B.H., J.T.P., and F.S.C. developed custom MATLAB scripts for analysis of electrophysiology studies. F.A. performed, analyzed, and interpreted kainic acid seizure challenge in mice. F.S.C., A.R.M., and A.C. performed immunohistochemistry of mouse tissue. Y.V., A.C., and F.S.C. performed, analyzed, and interpreted spatial transcriptomic study. J.T.P., A.V.M., E.A., and B.S.K. acquired funding. F.S.C. and J.T.P. discussed and interpreted all data with respective authors. F.S.C. and J.T.P. wrote the original draft of the manuscript, and all authors participated in manuscript revisions. **Competing interests:** The authors declare that they have no competing interests. **Data and materials availability:** All data associated with this study are present in the paper or the Supplementary Materials. Bulk transcriptomic data are available through GEO (accession number GSE203111). Correspondence and request for materials should be addressed to J.T.P.

Submitted 13 May 2021
Resubmitted 07 January 2022
Accepted 14 May 2022
Published 6 July 2022
10.1126/scitranslmed.abj4310

Science Translational Medicine

Enhancing GAT-3 in thalamic astrocytes promotes resilience to brain injury in rodents

Frances S. ChoIlia D. VainchteinYuliya VoskobiynykAllison R. MorningstarFrancisco AparicioBryan HigashikuboAgnieszka CiesielskaDiede W. M. BroekaartJasper J. AninkErwin A. van VlietXinzhu YuBaljit S. KhakhEleonora AronicaAnna V. MolofskyJeanne T. Paz

Sci. Transl. Med., 14 (652), eabj4310. • DOI: 10.1126/scitranslmed.abj4310

Halting astrocytes at the GAT3

Uncontrolled inflammation in the brain after an injury has been shown to contribute to increased seizure risk and cognitive impairments. The thalamus is a brain area particularly susceptible to damage after an injury. Here, Cho and colleagues showed that thalamic inflammation per se was sufficient to trigger the negative effects of brain injury by modulating the expression of the GABA-transported GAT3 in astrocytes. Restoring the expression of the GABA-transported GAT3 in this cell population reduced the negative outcomes associated with brain injury, suggesting that targeting astrocytes in the thalamus might be effective for preventing negative outcomes after brain injury.